Mid-Holocene thinning of David Glacier, Antarctica: Chronology and Controls

Jamey Stutz[1], Andrew Mackintosh[2], Kevin Norton[3], Ross Whitmore[1,2], Carlo Baroni[4], Stewart S.R. Jamieson[5], Richard S. Jones[2], Greg Balco[6], Maria Cristina Salvatore[4], Stefano Casale[4], Jae Il Lee[7], Yeong Bae Seong[8], Robert Mckay[1], Lauren J. Vargo[1], Daniel Lowry[1,9], Perry Spector[6], Marcus Christl[10], Susan Ivy Ochs[10], Luigia Di Nicola[11], Maria Iarossi[4], Finlay Stuart[11], and Tom Woodruff[12]

[1]Antarctic Research Centre, Victoria University of Wellington, PO Box 600, Wellington, New Zealand 6140
[2]School of Earth, Atmosphere and Environment, Monash University, 14 Rainforest Walk, Victoria, Australia 3800
[3]School of Geography, Earth and Environmental Sciences, Victoria University of Wellington, PO Box 600, Wellington, New Zealand 6140
[4]Dipartimento di Scienze della Terra, Università di Pisa, Via Santa Maria, 53, 56126 Pisa, Italy
[5]Department of Geography, Durham University, South Road, Durham, DH1 3LE, UK
[6]Berkeley Geochronology Center, 2455 Ridge Road, Berkeley, CA 94709, USA
[7]Korean Polar Research Institute, 26 Songdomirae-ro, Yeonsu-gu, Incheon 21990, Korea
[8]Department of Geography, Korea University,145 Anam-ro, Seongbuk-gu, Seoul, Korea
[9]GNS Science, 1 Fairway Dr. Avalon, 5010, New Zealand
[10]Department of Physics, ETH Zürich, Otto-Stern-Weg 5 8093 Zürich, Switzerland
[11]Scottish Universities Environmental Research Centre, Scottish Enterprise Technology Park/Rankine Av, Glasgow G75 0QF, United Kingdom
[12]PRIME Lab, Purdue University 525 Northwestern Avenue, West Lafayette, IN 47907, USA

Correspondence: Jamey Stutz (jamey.stutz@vuw.ac.nz)

Abstract. Quantitative satellite observations only provide an assessment of ice sheet mass loss over the last four decades. To assess long-term drivers of ice sheet change, geological records are needed. Here we present the first millennial-scale reconstruction of David Glacier, the largest East Antarctic outlet glacier in Victoria Land. To reconstruct changes in ice thickness, we use surface exposure ages of glacial erratics deposited on nunataks adjacent to fast flowing sections of David Glacier. We then use numerical modelling experiments to determine the drivers of glacial thinning.

Thinning profiles derived from 45 ^{10}Be and ^{3}He surface exposure ages show David Glacier experienced rapid thinning of up to 2 m/yr during the mid-Holocene ($\sim$6.5 ka). Thinning stabilised at 6 ka, suggesting the initial formation of the Drygalski Ice Tongue at this time. Our work, along with ice thinning records from adjacent glaciers, shows simultaneous glacier thinning in this sector of the Transantarctic Mountains occurred $\sim$3 ka after the retreat of marine-based grounded ice in the western Ross Embayment. The timing and rapidity of the reconstructed thinning at David Glacier is similar to reconstructions in the Amundsen and Weddell embayments.

To identify the drivers of glacier thinning along the David Glacier, we use a glacier flowline model designed for calving glaciers and compare modelled results against our geological data. We show that glacier thinning and marine-based grounding line retreat is initiated by interactions between enhanced sub-ice shelf melting and reduced lateral buttressing, leading to Marine Ice Sheet Instability. Such rapid glacier thinning events are not captured in continental or sector- scale numerical modelling

reconstructions for this period. Together, our chronology and modelling identify and constrain the drivers of a ~2,000-year period of dynamic glacier thinning in the recent geological past.

1 Introduction

Since the Last Glacial Maximum (LGM), ice sheets retreated in both hemispheres, causing a sea level rise of ~130 m (Clark et al., 2009). This period, the Last Glacial Termination, represents Earths last major period of climate warming between ~20 and 11.7 ka (Denton et al., 2010). Ice sheet retreat continued into the Holocene (11.7 ka-present), and global sea level stabilised at near preindustrial levels by 6-7 ka (Lambeck et al., 2014). During the Holocene, the Antarctic Ice Sheet (AIS) retreated from expanded positions on the continental shelf (Bentley et al., 2014). Ice sheet thinning and retreat was rapid at times, potentially contributing to periods of rapid sea level rise (Weber et al., 2014). However, quantitative age control on this retreat behaviour are only available for a limited number of sites in Antarctica, and are entirely absent from David Glacier, which is the focus of this study (Bentley et al., 2014; Small et al., 2019). Discovered by the British National Antarctic Expedition (1901-1904), David Glacier drains the East Antarctic Ice Sheet (EAIS), traverses and incises the Transantarctic Mountains (TAM) and discharges into the western Ross Sea as the floating Drygalski Ice Tongue (Fig. 1 and S1). Comprising an area ~210,000 km^2, the glacier is the largest in Victoria Land, representing a significant element of the Antarctic cryosphere, draining from Dome C and Talos Dome. Improved understanding of the timing and the processes that caused AIS retreat during deglaciation help us to better understand the processes driving observed mass loss in parts of Antarctica today.

Geological reconstruction of the AIS through time provides critical insights into the history of ice sheet change and can narrow uncertainty on Antarctica's contribution to global sea level rise. A geologic perspective on ice sheet behavior is particularly useful because:

1. Quantitative satellite observations only extend back ~40 years (IMBIE, 2018; IPCC, 2013; Miles et al., 2013; Rignot et al., 2019) and these observations do not fully capture natural variability of ice sheet behaviour.

2. Integration of the data constraining marine extent and terrestrial thickness of an ice mass through time provides a robust data set for evaluation of numerical ice sheet model simulations, which are used to predict future ice sheet contributions to sea level rise.

3. Recent studies of the complex interactions between the solid earth, cryosphere, and ocean highlight the need to understand short and long-term changes in the AIS (Barletta et al., 2018; Whitehouse et al., 2019; Meredith et al., 2019). Modern continuous GPS measurements of bedrock deformation record the integrated response to both modern and ancient ice mass change. The elastic component due to modern ice mass fluctuations can be modelled using satellite observations constraining ice mass balance. The viscous component represents a 'memory' of ice load history over cen-

turies to millennia. Ice load reconstructions constrained by cosmogenic dating of glacial samples provide a powerful tool to robustly model Glacial Isostatic Adjustment (GIA), a complex suite of ice sheet-bedrock-sea level feedbacks critical for projections of future global sea level.

Reconstructions of large marine terminating outlet glaciers provide an opportunity to constrain and understand the terrestrial and marine sectors of ice sheets. At the LGM, the David Glacier thickened and expanded as an ice stream, coalesced with grounded marine-based ice, and extended hundreds of kilometres into the western Ross Sea (Anderson et al., 2014; Livingstone et al., 2012; Shipp et al., 1999). During deglaciation, grounding line retreat from north of Coulman Island was initiated by ∼13 ka, with retreat near Terra Nova Bay (TNB) by ∼11 ka (Licht et al., 1996; Domack et al., 1999; McKay et al., 2008). Subsequent grounding line retreat north of Ross Island was achieved by ∼8.6 ka and a modern configuration established by ∼2-4 ka (Anderson et al., 2014; McKay et al., 2016). Outlet and valley glaciers along the Northern Victoria Land sector (Reeves, Priestley, and Tucker, Aviator, Campbell glaciers, respectively) began thinning at ∼17 ka and the majority of thinning ceased by ∼7.5 ka, broadly coincident with a linear rise in sea level and ocean temperatures throughout deglaciation (Baroni and Hall, 2004; Johnson et al., 2008; Smellie et al., 2018; Goehring et al., 2019; Rhee et al., 2019). In contrast, outlet glaciers covering a large swath of the TAM from Southern Victoria Land to Southern TAM, experienced episodic thinning during the early-mid Holocene, likely due to local topographic effects associated with Marine Ice Sheet Instability (Jones et al., 2015; Spector et al., 2017). Along the Transantarctic Mountains, mid-Holocene outlet glacier thinning and retreat occurred during a relatively stable period of air temperature and sea level after the majority of post-glacial sea level rise and rising atmospheric temperatures occurred (Lambeck et al., 2014; Jones et al., 2015; Spector et al., 2017; Jones et al., 2020). Overall, variation in the timing of glacier thinning suggests sea-level rise, ocean warming, and overdeepened subglacial topography controlled the reconstructed glacier behaviour.

Glacial reconstructions based on marine geological and geophysical data from the western Ross Sea focus on tracking a grounding line that represents sector-wide ice sheet change (Licht et al., 1996; Domack et al., 1999; Shipp et al., 1999; McKay et al., 2008; Anderson et al., 2014). However, there is increasing evidence that palaeo-ice streams and TAM outlet glaciers decoupled from the larger ice sheet occupying the Ross Embayment during deglaciation (Halberstadt et al., 2016; Lee et al., 2017). As the grounding line retreated southward, local subglacial topography is thought to have influenced local glacier thinning and retreat rates (McKay et al., 2016; Halberstadt et al., 2016; Jones et al., 2015, 2021).

Marine geophysical and geological data reveal a large grounding zone wedge (GZW) near Coulman Island, marking the probable maximum limit of grounded ice in the Ross Seea during the LGM (Shipp et al., 1999). Based on marine sedimentary analysis and radiocarbon age dating, the timing of retreat from the Coulman Island GZW initiated at ∼13 ka, punctuated by few short periods of staggered retreat through the deep Drygalski Trough (Licht et al., 1996; Domack et al., 1999; Anderson et al., 2014; Yokoyama et al., 2016). By ∼10 ka, ^{14}C dating of acid insoluble organic (AIO) matter from sediment cores, suggest the grounding line in the Ross Sea migrated south of the David Glacier (Licht and Andrews, 2002). However, AIO dates in the Ross Sea are known to be unreliable due to potential input of anomalously old carbon by reworking, and this 10 ka constraint is likely to represent a maximum age of this retreat (Andrews et al., 1999; Rosenheim et al., 2013). Furthermore, short pauses

in onshore thinning may be temporally linked to short periods of stability recorded by small grounding zone wedges deep in the Drygalski Trough and near TNB (Brancolini et al., 1995; Anderson et al., 2014; Lee, 2019).

Marine sedimentary records from the deepest parts of the inner Drygalski trough provide evidence of a lingering ice shelf, but anomalously old surface ^{14}C ages hinder coherent chronologies (Licht et al., 1996; Frignani et al., 1998; Domack et al., 1999; Licht and Andrews, 2002; Prothro et al., 2020). North of TNB, meteoric ^{10}Be and compound specific radiocarbon ages capture the retreating calving line and onset of open marine conditions by 8 ka (Yokoyama et al., 2016). This timing is consistent with the raised beach chronology of Baroni and Hall (2004), which marks the local onset of coastal open marine conditions no later than 8 ka.

Surface exposure dating using *in situ* terrestrial cosmogenic nuclides has transformed the ability to reconstruct the AIS through time (e.g., Stone et al., 2003; Mackintosh et al., 2007; Todd et al., 2010; Balco, 2011; White et al., 2011; Jones et al., 2015; Spector et al., 2017; Small et al., 2019). Through surface exposure dating of glacial deposits, this study aims to constrain the LGM to present behaviour of the David Glacier. Guided by our resulting ice thinning histories, we investigate the forcings and controls on glacier thinning using a glacier flowline model. We use geologic data and ice sheet model outputs to frame and inform the first detailed deglacial sensitivity experiments for David Glacier, building on previous flowline modelling approaches in Antarctica (Jamieson et al., 2012; Jones et al., 2015; Whitehouse et al., 2017).

2 Methods

2.1 Field and laboratory methods

In the field, we collected erratics and glacially striated bedrock adjacent to the David Glacier both upstream and downstream of the present-day grounding line. Downstream sites, Hughes Bluff and D'Urville Wall, are expected to show the most recent and dramatic change while the upstream site, Mt. Kring, is expected to record smaller and longer term changes in ice thickness (Fig.1) (Anderson et al., 2004; Bockheim et al., 1989). Using the structure from motion photogrametry technique (Vargo et al., 2017), we use helicopter based photography to construct a high-resolution digital elevation model of each field site allowing integration of glacial geological field surveys with the regional and local geomorphology (Baroni et al., 2004) (Figs.S3 and S4).

We primarily sampled glacial erratic cobbles from local glacial deposits and glacially moulded bedrock surfaces along vertical transects perpendicular to the modern glacial flow direction. The cosmogenic nuclide inventories in cobbles and bedrock comprise signals of both exposure since the most recent deglaciation, and nuclides accumulated during any prior exposure (known as 'inheritance'). For long-lived nuclides such as ^{10}Be, this inherited component can be significant (Sugden et al., 2005; Balco, 2011). Inheritance of cosmogenic nuclides is widespread in Antarctica as the cold-based nature of some ice acts to cover (preventing build up of cosmogenic nuclides) without causing sufficient erosion (Sugden et al., 2005; Atkins, 2013) . However, since cosmic rays attenuate rapidly with depth into rock, subglacial erosion of more than a few meters can reset the cosmic-ray signal. As such, we primarily focused on sampling faceted and striated glacial erratics because they indicate a subglacial origin which reduces the likelihood of a prior exposure history and these intact features indicate minimal

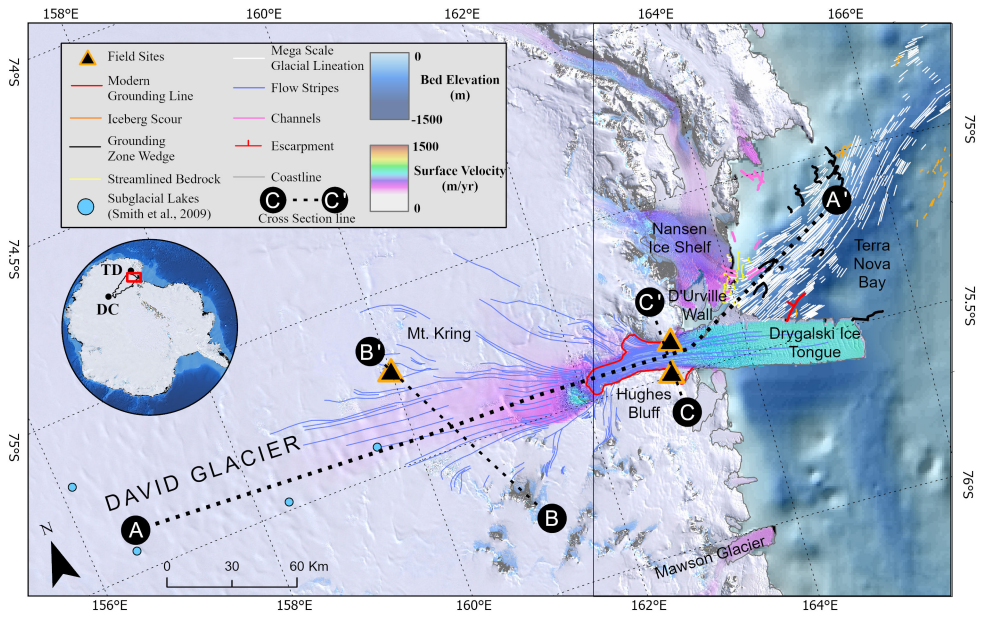

Figure 1. Map of greater David Glacier/ Terra Nova Bay region including mapped sub-marine geomorphic features and geographic features mentioned in text. Geomorphic cross sections (A-A', B-B' and C-C') highlighted in Fig. S1. Inset shows extent of main map along with drainage basin of David Glacier and position of two local ice domes: Dome C (DC) and Talos Dome (TD). Data sources: Satellite imagery of (Bindschadler et al., 2008), surface velocity of (Rignot et al., 2011), surface elevation of (Howat et al., 2019), bed elevation of (Fretwell et al., 2013) and bathymetry of (Arndt et al., 2013)

post-depositional erosion. Exposure ages from these samples are interpreted to track glacier thinning at the site because such samples would have been elevated to the former ice margin prior to deposition (Stone et al., 2003; Mackintosh et al., 2007; Jones et al., 2015; Small et al., 2019).

In this study, we use cosmogenic nuclides ^{10}Be and ^{3}He to determine surface exposure ages on 45 samples. For ^{10}Be analysis, quartz is the target mineral and is present in granites and sandstones. For ^{3}He, pyroxene is the target mineral and present in dolerites. In the field, we preferentially sampled on isolated, local topographic high points, distant from areas of blue ice, snow drifts or local till deposits. While it is the focus of this study to use glacial erratics to track glacier thinning, we also collected bedrock samples to better understand complex exposure histories due to burial and non-erosive nature of cold-based ice (Atkins, 2013; Joy et al., 2014).

Samples collected in the field were processed at the cosmogenic nuclide facilities at Te Herenga Waka Victoria University of Wellington. For ^{10}Be, we separated quartz by crushing and sieving to extract the 250-500-micron grain size fraction. Magnetic minerals were separated using a Frantz isodynamic magnetic separator. For granitic rocks, feldspars were removed by froth

flotation. We etched samples for one day in 10% Hyrdochloric acid, for one day in 2.5% Hydroflouric acid (HF) and 3 days in 1%HF to further purify the quartz separates. Beryllium was extracted from quartz following an established method including the addition of a ^{9}Be carrier, enhanced quartz etching and digestion followed by ion exchange chromatography and BeOH precipitation (Norton et al., 2008). Targets of BeO were packed and sent to the Purdue Rare Isotope Measurement Laboratory (PRIME lab) for analysis using accelerated mass spectroscopy (AMS). For ^{3}He, we targeted pyroxene from the 125-250 micron grain size fraction. Pure pyroxene was obtained using an established HF etching method and ^{3}He/^{4}He ratios were measured at the Berkeley Geochronology Center noble gas spectrometer (Bromley et al., 2014; Blard et al., 2015; Balter-Kennedy et al., 2020). We supplemented this data set with eight samples collected prior to the 2016-17 austral summer and those samples were processed for^{10}Be or ^{3}He using methods outlined in Oberholzer et al. (2003, 2008) and Di Nicola et al. (2009, 2012). Exposure ages are calculated by converting the AMS derived ^{10}Be/^{9}Be ratio to ^{10}Be concentration by subtracting a known amount of ^{9}Be carrier added during chemical processing. Final exposure ages are calculated using ^{10}Be or ^{3}He concentration, field information (elevation, shielding, and sample thickness) and production rate scaling method (LSDn) (Balco et al., 2008; Lifton et al., 2014; Marrero et al., 2016; Jones et al., 2019). For ^{10}Be, we employed Jones et al. (2019) systematics (http://ice-tea.org/en/) and for ^{3}He, we use Balco et al. (2008) systematics (https://hess.ess.washington.edu/). All relevant data used to calculate exposure ages are served on the ICE-D online database (Balco, 2020) within the David Glacier region (antarctica.ICE-D.org) and in supplemental data Tables 1-5. The resulting glacier thinning chronologies derived from surface exposure ages inform our glacier modelling approach by providing geometric targets for evaluating the simulated maximum thickness of ice, and the subsequent magnitude and duration of glacier thinning.

2.2 Glacier modelling approach

To understand potential controls on the grounding line migration and onshore thinning, we apply a glacier flowline model to the David Glacier. Originally designed to track grounding line migration using a moving grid, the flowline model we employ has been described fully elsewhere (e.g. Vieli and Payne, 2005; Nick et al., 2009; Jamieson et al., 2012; Enderlin et al., 2013; Jamieson et al., 2014; Clason et al., 2016; Whitehouse et al., 2017). The underlying theory and governing equations are outlined in Vieli and Payne (2005) and here we describe the components pertinent to our research questions.

Our glacier modelling focuses on a ~1,600 km long flowline from Dome C to western Ross Sea shelf edge. The domain consists of varying flow regimes and extends to areas where the ice stream converged with grounded ice in the western Ross Embayment during the LGM. Ice flow is governed by fundamental equations 1 - 6.

Ice flow along the grounded portion of the model domain, u, is calculated using the shallow ice approximation which assumes ice flow only from internal ice deformation and horizontal velocity defined as:

$$u = C\left(\frac{\delta s}{\delta x}\right)h^{n+1} \tag{1}$$

where n (=3) is Glen's flow law exponent, s is ice surface elevation, h is ice thickness and C is a constant given by:

$$C = \frac{2A(\rho_i g)^n}{n+2} \tag{2}$$

As ice reaches flotation, ice is assumed to spread unidirectionally along the flowline, ice flow is balanced by:

$$2\frac{\delta}{\delta x}hv\frac{\delta u}{\delta x} = \rho_i g h \frac{\delta s}{\delta x} \tag{3}$$

where ρ_i is ice density (0.910 g/cm^3), g is gravitational acceleration (9.8 m/s^2) and v is the vertically average effective viscosity defined as:

$$v = A^{\frac{-1}{n}} \left[\left(\frac{\delta u}{\delta x} \right)^2 \right]^{(1-n)/(2n)} \tag{4}$$

Where A is the temperature dependant rate factor (for -20°C) and $\frac{\delta u}{\delta x}$ is the effective strain rate.

For an ice stream, equation 4 is modified by including a basal friction coefficient β which is linearly related to the horizontal velocity u and is given by:

$$2\frac{\delta}{\delta x}hv\frac{\delta u}{\delta x} - \beta^2 u = \rho_i g h \frac{\delta s}{\delta x} \tag{5}$$

Recent applications using this model include testing the impact of a width term to calculate lateral buttressing along a coupled ice stream-shelf and enhanced treatment of ice shelf dynamics. Nick et al. (2010) and Jamieson et al. (2012) modelled depth (H) and width (W) averaged ice flow (u) using the following equation:

$$2\frac{\delta}{\delta x}hv\frac{\delta u}{\delta x} - \beta^2 u + \frac{H}{W}\left(\frac{5u}{2AW} \right)^{\frac{1}{n}} = \rho_i g h \frac{\delta s}{\delta x} \tag{6}$$

The inclusion of the width term allows modelling of changing offshore trough width which is common in palaeo-ice streams and outlet glaciers, and further supported by geomorphic interpretations using high resolution bathymetry data (Jamieson et al., 2012; Livingstone et al., 2012, 2016). For this study, we map all geomorphic features using the global multi-resolution topography data set within GeoMapApp (geomapapp.org) based on analogs (Dowdeswell et al., 2016) and prior regional mapping (Stutz, 2012; Shipp et al., 1999; Anderson et al., 2014; Halberstadt et al., 2016).

Whitehouse et al. (2017) improved the ice shelf dynamics to incorporate the treatment of large horizontal grounding line movements that are expected for the palaeo-David Glacier based on the long term presence of the Drygalski Ice Tongue and evidence of extensive sub-ice shelf conditions inferred from marine sedimentary cores (Domack et al., 1999; McKay et al., 2008). In the model, the ice shelf geometry evolves with time, and variations in ice shelf thickness and extent are fed into lateral drag calculations (Whitehouse et al., 2017). Improved treatment of ice shelf dynamics allows exploration of the grounding line sensitivity to ice shelf feedbacks associated with marine ice sheet instability. Importantly for this study, a reduction in lateral buttressing from adjacent, coalesced ice is expected as the expanded David Glacier and grounded ice in the Ross Sea decouple, which has been suggested from interpretation of submarine geomorphic features in the western Ross Sea (Shipp et al., 1999; Halberstadt et al., 2016).

2.2.1 Boundary conditions

The model domain, sampled at 5 km resolution, runs along a ∼1,600 km flowline from Dome C to the continental shelf break (Fig. 2 and Fig. S6). Fig 1 and Fig. S1 provide map extent of cross section views detailing the subglacial topography surrounding the modern day grounding line. In order to simplify the flowline domain, we focus on the dominant ice stream emanating from Dome C. Using standard basin delineation tools in ArcGIS, we construct a drainage basin outline from surface elevation and ice velocity (Rignot et al., 2011; Howat et al., 2019). We follow on to construct a flowline (centre of ice stream) and flowline-parallel width across the onshore domain using derived products from the ArcGIS basin delineation tools. The marine sector of the flowline follows the Drygalski Trough axis and runs parallel to mapped mega-scale glacial lineations (MSGL) and we determine the ice stream width by orientation and distribution of trough parallel MSGLs consistent with Jamieson et al. (2012). The ice stream width parallel to the model flowline controls the lateral stress applied by coalesced ice along the flowline (Equation 6).

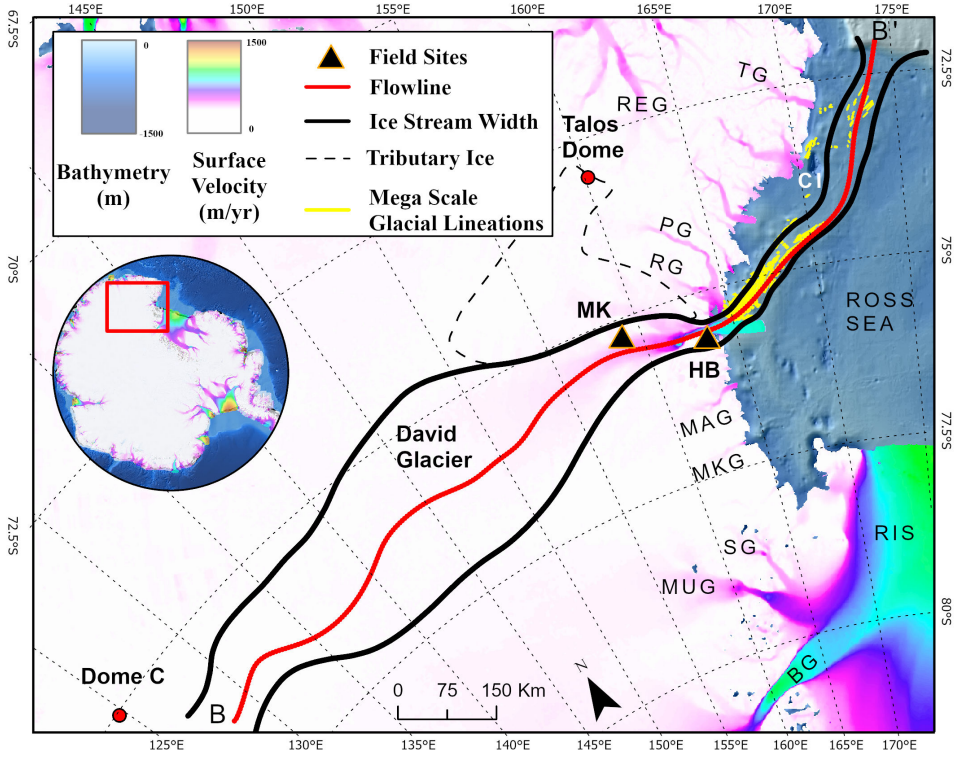

Figure 2. Map of model domain with modern ice surface velocity of Rignot et al. (2011) and bathymetry of Arndt et al. (2013). Flowline follows red line, ice stream width in black. RIS: Ross Ice Shelf, BG: Byrd Glacier, MUG: Mulock Glacier, SG: Skelton Glacier, MKG: Mackay Glacier, MAG: Mawson Glacier, RG: Reeves Glacier, PG: Priestley Glacier, AG: Aviator Glacier TG: Tucker Glacier, CI: Coulman Island, HB: Hughes Bluff, MK:Mt. Kring

In order to evaluate model performance and appropriate boundary conditions for deglacial experiments, we tune user defined parameters to reproduce the modern behaviour of the David Glacier. The model allows the user to input surface and bed geometry, ice stream width, accumulation, velocity and a basal traction parameter. Modern surface elevation, surface mass balance and ice velocity are well constrained from satellite and *in situ* measurements (Rignot et al., 2011; van Wessem et al., 2018; Howat et al., 2019). In order to account for confluent ice from tributary glaciers we employ an ice mass accumulation scheme used in previous modelling studies whereby tributary ice mass is added along the length of the ice stream (Jamieson et al., 2014; Whitehouse et al., 2017). This tributary 'injection' from a secondary ice stream originating from Talos Dome is included in the surface mass budget and for the David Glacier model domain (Fig. 2).

Ongoing aerogeophysical and remote sensing techniques continue to reveal new detail of the subglacial environment of the AIS (Schroeder et al., 2020; MacGregor et al., 2021). Common among many TAM outlet glaciers, a prominent bedrock high immediately upstream of the modern grounding line provides a significant stabilising impact on the David Glacier (Fretwell et al., 2013; Morlighem et al., 2019). The bed geometry along the flowline is derived solely from Bedmap2 and the International Bathymetric Chart of the Southern Ocean (Fretwell et al., 2013; Arndt et al., 2013).

Geologic data from former glaciated terrains and satellite observations can be used to approximate basal conditions, yet a general lack of *in situ* data from the ice sheet basal environment lead to enduring uncertainties in the basal stress regime (Joughin et al., 2006; Stokes et al., 2015). Based on existing knowledge of sea floor morphology and consistent with previous modelling experiments, the basal traction parameter used in this model attempts a first order approximation of two subglacial basal environments: 1) relatively high basal traction for onshore ice flow over bedrock and 2) relatively low basal traction for offshore ice flow over soft sediments associated with basal till deposits (Dowdeswell et al., 2004; O Cofaigh et al., 2005).

We use modelled surface mass balance (van Wessem et al., 2018), calculated sub-ice shelf melt rate (SIMR) (Wuite et al., 2009) and modern geometry (Howat et al., 2019; Fretwell et al., 2013) to set the model up so that it replicates modern flow conditions and geometry at a steady state (Table 1). We then tune the basal traction parameter so that we end up with a relatively stable ice thickness and velocities. The model is unable to reproduce stable conditions along the steep surface profile as the David Glacier descends from the ice sheet interior. In this zone, the modelled upper surface is steep and undergoes thinning throughout the modelled time period. In an effort to stabilise the upper ice surface upstream of the grounding line, we tune the basal traction parameter, effectively stiffening the bed, to reduce the modelled instability. We note here that, according to equation 5, as the ice surface evolves, basal traction evolves naturally; for example, as the ice profile gets steeper or thicker, the basal traction evolves. Resultant modelled estimates of basal shear stress approach 100 kPa in this setting. While difficult to constrain with *in situ* measurements, Zoet et al. (2012) suggest higher stresses should be expected near the modern day grounding zone which is consistent with the modelled stress distribution in this study. Overall, the modern grounding line position, ice shelf thickness and ice shelf length are stable over a 2,000 year modelled period.

2.2.2 Deglaciation approach

LGM geometric boundary conditions incorporate modelled ice thickness and surface velocity from W12, an ice sheet reconstruction based on available geologic data (Fig.S6) (Whitehouse et al., 2012). Using the W12 modelled ice thickness and

Parameter	Modern Conditions	Deglacial Conditions
Ice temperature	-20	-25
Max SIMR	-5	-1 to -11
Accumulation rate (% RACMO2)	100	75

Table 1. Parameter values used for model tuning approach and deglacial sensitivity experiments. SIMR=sub-ice shelf melt rate. Accumulation values reported as percentage of RACMO2 (van Wessem et al., 2018)

modern bed elevation (Fretwell et al., 2013) allows for a calculated estimate of upper ice surface without introducing uncertainty involving variable along flow isostatic response and dynamic topography associated with the long-term evolution of the Antarctic subglacial topography (Stern et al., 2005; Whitehouse et al., 2019; Paxman et al., 2019). We do not compare our sensitivity experiments results with those of W12 ice reconstruction, we purely use a calculated upper ice surface as a starting point for our model during spin up. The resulting ice thickness geometrically fits to geologic data (i.e. covers highest elevation Holocene aged erratics) and serves as an initial ice profile for deglaciation sensitivity experiments.

In order to account for environmental changes during deglaciation, transient changes in accumulation and internal ice temperature are tuned over the modelled period to ensure a stable LGM configuration consistent with geological constraints. Knowledge of past accumulation over glacial-interglacial cycles are restricted to ice core data and internal ice sheet layer mapping near high elevation ice domes (Siegert, 2003; Frezzotti et al., 2005; Buiron et al., 2011; Cavitte et al., 2018). Generally, modern accumulation patterns show relatively low accumulation (0.02 m/yr) over the East Antarctic interior and high accumulation (0.2 m/yr) near the coastline (Arthern et al., 2006; Lenaerts et al., 2012; van Wessem et al., 2018). Interpretations from ice core records suggest LGM accumulation rates were lower than modern accumulation rates and generally correlate well with temperature proxy records throughout the Holocene (Siegert, 2003; Veres et al., 2013). We use a scaling relationship between modern accumulation patterns and estimate that accumulation at $\sim$15 ka was roughly 75% of modern accumulation (Veres et al., 2013). For internal ice temperature, we increase this value through time to represent the increase in temperature that occurred during deglaciation. The internal ice temperature that deglaciation is not known and for this study, we used values of -25°C for the first 7,500 model years to -20°C during the remaining 7,500 model years. By accounting for changes in accumulation rate and internal ice temperatures during deglaciation, we are able to demonstrate these were not responsible for driving modelled grounding line retreat.

Deglacial sensitivity experiments designed to understand the controls on thinning and retreat are initialised with a set of user defined parameters derived from modern basal traction tuning. Using an optimised set of accumulation and internal ice temperature forcings (Table 1), we explore transient changes in lateral buttressing reduction (LBR) and sub-ice shelf melt rates (SIMR) to isolate their relative influence on glacier thinning and retreat.

LBR and SIMR are the only two forcings we investigate as regional proxies for internal ice temperature and accumulation (only two other user defined forcings for this model) are poorly constrained and show relatively minor variation over the Holocene (Buiron et al., 2011; Verleyen et al., 2011). During the LGM, the David glacier coalesced with grounded ice in the Ross Sea and was thus, susceptible to ocean-driven basal melt as well as changes in lateral drag (buttressing) from surrounding grounded ice. We initiate grounding line retreat by progressively increasing SIMR or decreasing lateral buttressing. For combined forcing experiments (MS1-3), we use a melt rate and progressively reduce lateral buttressing until the grounding line retreats to near modern configuration. We introduce a one kyr timing lag between SIMR forcing and LBR. This staggered forcing, particularly in the combined forcing experiments, seeks to simulate ocean-driven melt occuring first followed by a reduction in lateral buttressing. This scenario is designed to represent a 'calving bay' environment, potentially led by ocean heat driven sub-ice shelf melt, as recognised in western Ross Sea (Domack et al., 1999, 2003, 2006) and East Antarctic margin (Leventer et al., 2006; Mackintosh et al., 2014)

All sensitivity experiments run for 15 kyr with an initial spin up period lasting 7.5 kyr for SIMR forcing and 8.5 kyr for LBR forcing, at which point a forcing perturbation is applied for the remaining modelled period. We run our experiments for 15 kyr to provide ample spin up time at glacial conditions and force our model from 7.5 kyr to explore forcings that, by the end of the modelled period, result in a configuration consistent with modern observations. When forcing the model, we linearly increase the forcing over a 500 year period. In SIMR cases, we varied the SIMR perturbation within a 0.5 m/yr window at 500 year temporal frequency in order to simulate short-lived pulses of relatively warmer or cooler water mass changes. Further, it is not the intention of these sensitivity experiments to reproduce the exact timing of marine-based grounding line retreat, but rather, we aim to explore the range of possible drivers that would enable the overall scale of retreat observed to present day. All idealised scenarios are presented in Table 2.

3 Results chronology

Of the 45 samples analysed in this study, 21 yield mid-Holocene exposure ages. Holocene aged samples are interpreted to have received minimal prior exposure (i.e. inheritance) and suggest a simple exposure history. Focusing on two sites, we derive a high-resolution chronology of glacier thinning from Mt. Kring and Hughes Bluff.

3.1 Mt. Kring

Mt. Kring, situated in the interior of the EAIS, flanks the streaming ice of David Glacier draining Dome C. The nunatak, composed of layered dolerite, stands ~300 metres above the modern ice surface, henceforth 'above the ice'. Of the 24 samples processed, three are dolerite bedrock and 21 erratics of mixed lithologies (Fig. 3 and S3). The surface at the peak of Mt. Kring lacks glacial striations or erratics and has an apparent ^{3}He bedrock exposure age of 554 $\pm$ 91 ka. A discontinuous, steep ridge line between ~200-300 metres above the ice was not sampled due to inaccessibility. At ~200 metres above the ice, the bedrock is striated parallel to the modern ice flow direction and has an apparent ^{3}He exposure age of 550 $\pm$ 82 ka. The highest elevation erratic is found at ~180 metres above the ice with increasing erratic abundance culminating in a drift sheet covering

Deglacial Experiments	SIMR (m/yr)	LBR (%)
M1	-1 / -1.5	0
M2	-1 / -2	0
M3	-1 / -11	0
S1	-1	0 / 0
S2	-1	0 / 4
S3	-1	0 / 40
MS1	-1 / -5	0 / 40
MS2	-1 / -7	0 / 30
MS3	-1 / -9	0 / 26

Table 2. Idealised deglacial sensitivity experiments. Sub-ice shelf melt rate (SIMR) varies within a 0.5 m/yr window around value reported. SIMR is forced at 7,500 model years and lateral buttressing reduction (LBR) is forced at 8,500 model years. X / Y indicates initial conditions and forced conditions, respectively. If held constant, one value is reported.

nearly all bedrock below ∼110 metres above the ice. Striated, bulleted cobbles and boulders of dolerite, basalt and sandstone are common in the thin, patchy drift covering the bedrock. Based on our erratic exposure dating, the glacial drift here is a composite of three age populations (Fig. 4A). The younger population spans from 7.4-5.5 ka (^{10}Be, n=5)(Fig. 4B). The older population spans from 51-25 ka (^{10}Be, n=8 and ^{3}He, n=4). The oldest erratic age population shows scattered evidence of glacial behavior between 123-63 ka (^{10}Be, n=2,^{3}He, n=2). The older populations are likely an artifact of repeated burial by overriding ice and multiple periods of exposure (i.e. inheritance).

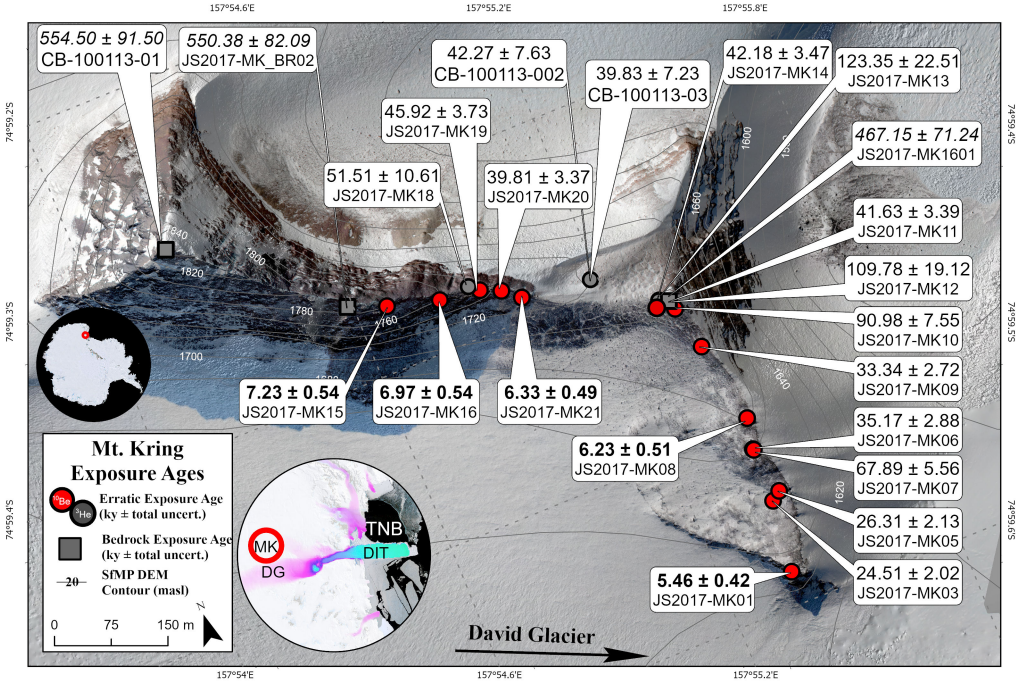

Figure 3. Orthomosaic map of Mt. Kring with all exposure ages, ^{10}Be (red) and ^{3}He (grey), and total errors. Erratics and bedrock ages plotted as circles and squares, respectively. Bold ages indicate Holocene age erratics and italicised ages indicate bedrock exposure. Large inset displays surface velocity of (Rignot et al., 2011) and small inset displays LIMA data of (Bindschadler et al., 2008). DG=David Glacier, DIT=Drygalski Ice Tongue, TNB=Terra Nova Bay and MK=Mt. Kring

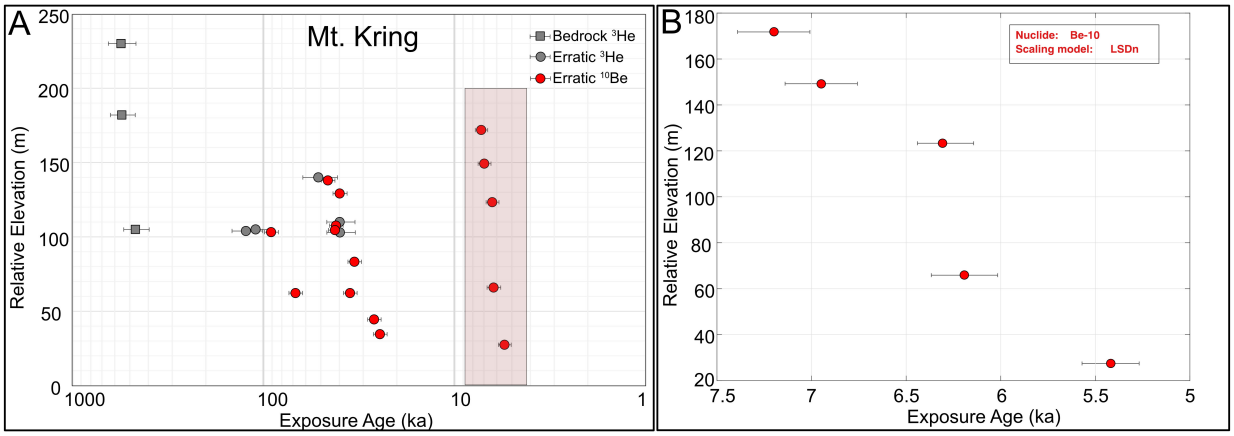

Figure 4. Relative elevation, above the ice, vs calculated surface exposure ages for Mt. Kring. (A) All exposure ages. Erratics plotted as circles, bedrock as squares(^{10}Be, red and ^{3}He, grey). Errors bars show total uncertainty. (B) Shows only Holocene ages.

3.2 Hughes Bluff

Hughes Bluff, situated on the Scott Coast, is a granite outcrop along the southern flank of the David Glacier. The outcrop is glacially scoured exhibiting spectacular rochés moutonnées, crescentic gouge marks and striations parallel to modern flow directions (Fig. 5 and Fig. S4). Scattered glacial erratics blanket the entire outcrop. ^{10}Be exposure ages from 15 erratics span from 6.7-4.3 ka (Fig. 6). The majority of glacial erratics are dated to between 6.7 and 6.2 ka. Two bedrock surface exposure ages from the highest and lowest outcrops (20.55 ka $\pm$ 2.10, 5.5 $\pm$ 0.47 ka) suggest significant wet-based glacial erosion since the LGM. At 20 metres above the ice, similar bedrock and erratic ages provide evidence of recent emergence of this low-lying outcrop since 5.5 ka. Hughes Bluff displays extensive glacial erosion which suggests the ice thickness at the LGM was considerably greater than 230 m, the maximum elevation at Hughes Bluff (Frisia et al., 2017). While the onset and magnitude of thinning prior to 6.7 ka is not constrained, the Hughes Bluff chronology clearly indicates a period of rapid ice surface lowering during the mid-Holocene.

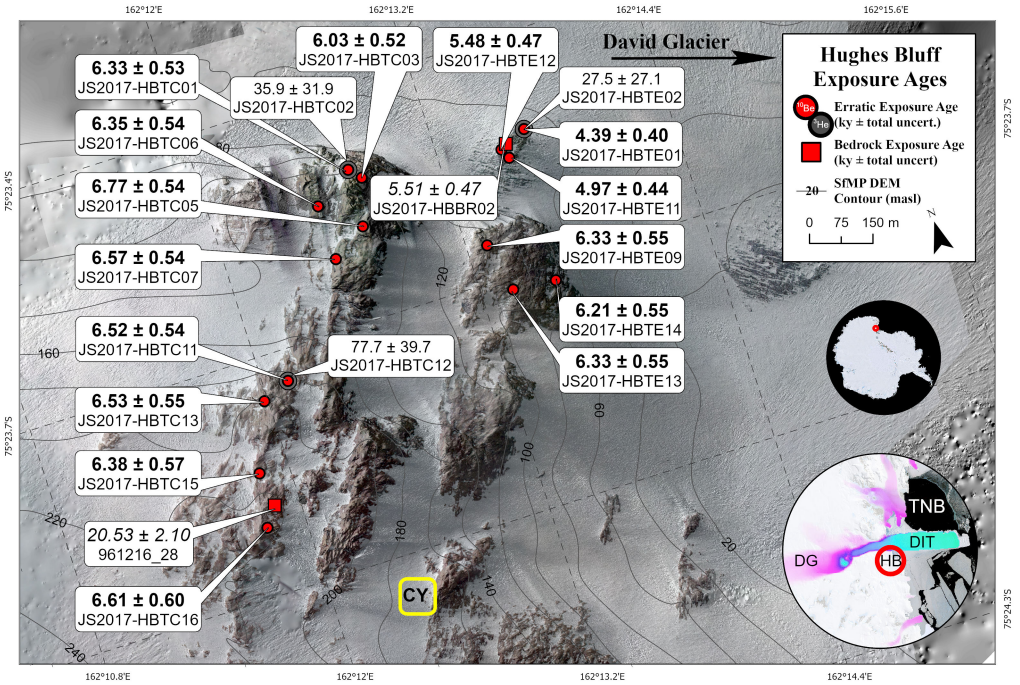

Figure 5. Orthomosaic map of Hughes Bluff with all exposure ages, ^{10}Be (red) and ^{3}He (grey), and total errors listed. Erratics and bedrock ages plotted as circles and squares, respectively. Bold ages indicate Holocene age erratics and italicised ages indicate bedrock exposure. Large inset shows surface velocity of (Rignot et al., 2011) and small inset shows LIMA data of (Bindschadler et al., 2008). DG=David Glacier, DIT=Drygalski Ice Tongue, TNB=Terra Nova Bay, HB=Hughes Bluff and CY= Camp Yellow

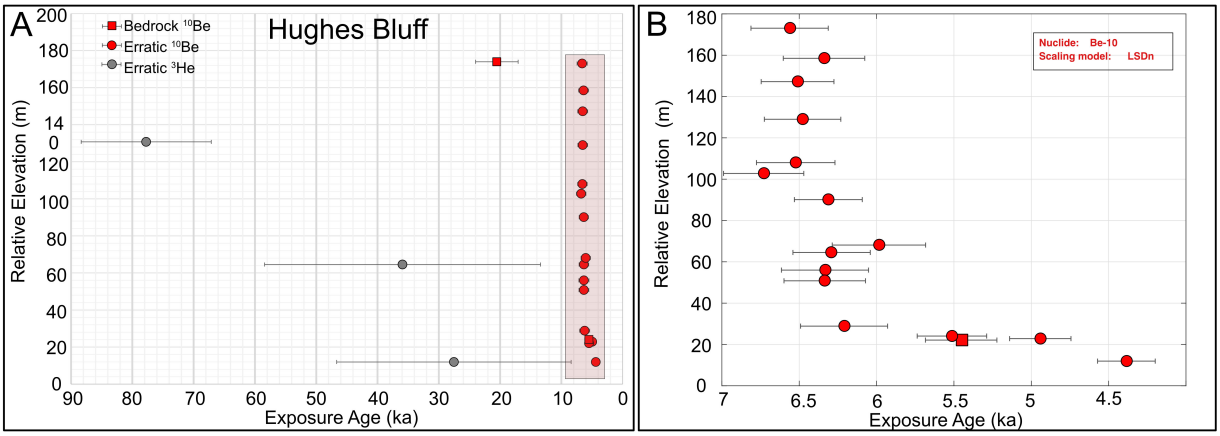

Figure 6. Relative elevation, above the ice, vs calculated surface exposure ages for Hughes Bluff (A) All exposure ages. Erratics plotted as circles, bedrock as squares (^{10}Be, red and ^{3}He, grey). Errors bars show total uncertainty. (B) Shows only Holocene ages.

3.3 High elevation constraints

In an effort to identify higher elevation glacial activity and long-term erosion history, field work was undertaken along the D'Urville Wall and Mt. Neumayer area (Fig. S5). The D'Urville Wall is a steep, high-elevation (>400 metres above the ice) granite outcrop delimiting the northern flank of David Fjord. The geomorphology and exposure ages from two field sites situated high above the David Glacier (Mt. Neumayer and Cape Phillipi) limit the reconstruction of the upper glacier surface during the LGM. Mt. Neumayer extending above the D'Urville Wall forms a rounded summit with faint striations sub-parallel to modern ice flow with few scattered erratics (Baroni et al., 2004). In areas 400 metres above the ice, bedrock samples contain weathering rinds and deep weathering pits filled with erratics (Baroni et al., 2004; Giorgetti and Baroni, 2007). Bedrock exposure ages from Mt. Neumayer (649 metres above the ice, 642 ± 61 ka), a terrace on top of the D'Urville Wall (418 above the ice, 116 ±10 ka) and Cape Phillipi (∼300 metres above the ice, 532 ±52 ka, 957 ±98 ka) suggest either a thin cover of cold based ice or ice free conditions through the LGM. High elevation bedrock samples are much younger than exposure ages from nearby bedrock at similar height above the ice and suggests burial by non-erosive ice (Di Nicola et al., 2012). Taken together, these bedrock exposure ages likely imply that the LGM ice surface along the northern flank of David Glacier was between 300 and 649 metres higher than today. This estimate is supported by geomorphic evidence from Hughes Bluff, which indicates ice thicker than 230 m, broadly consistent with the LGM elevation of ∼400 masl derived from drift deposits in TNB (Stuiver et al., 1981; Orombelli et al., 1990; Di Nicola et al., 2009) (Fig. S2).

3.4 Palaeo-thinning rates

Using the high-resolution chronology from Hughes Bluff and Mt. Kring, we derive a mean estimate of palaeo-thinning rates along David Glacier using a weighted least squares regression scheme within the iceTEA plotting tools (www.ice-tea.org) (Jones et al., 2019). These reconstructed glacier thinning rates are compared to modern thinning rates derived from satellite data

and continental-scale ice sheet models (Small et al., 2019). At Mt. Kring, we reconstruct a 2 ka thinning event from 7.5-5.5 ka of up to 0.19 m/yr (0.06-0.19, 2σ) thinning rate (Fig. 7A). At Hughes Bluff, we reconstruct a period of rapid thinning from 6.7-6.2 ka of up to 2 m/yr (0.19-2.06 m/yr, 2σ) followed by $\sim$4 kyr period of minimal thinning (Fig. 7B). The reconstructed palaeo-
325 thinning along the David Glacier during the mid-Holocene is synchronous with rapid thinning reconstructed at a number of sites in the Weddell embayment (Nichols et al., 2019; Johnson et al., 2019; Small et al., 2019; Bentley et al., 2017), Amundsen Sea Sector (Johnson et al., 2008, 2014, 2017), Marie Byrd Land (Stone et al., 2003), and the Transantarctic Mountains (Todd et al., 2010; Jones et al., 2015; Spector et al., 2017; Jones et al., 2020). However, the rate of palaeo-thinning reconstructed at Hughes Bluff is one of the highest rates recorded in Antarctica, comparable to a reconstruction from nearby Mackay and
330 Mawson Glaciers (Small et al., 2019; Jones et al., 2015, 2020).

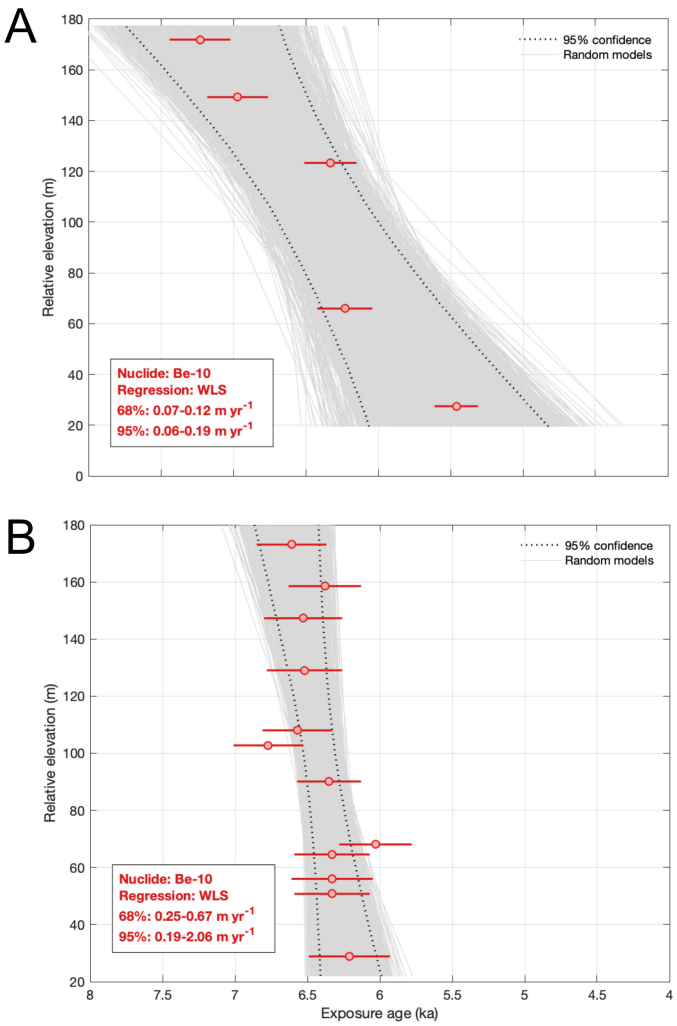

Figure 7. Linear thinning rates derived from relative elevation, above the ice, and mid-Holocene exposure ages estimated using ice-tea.org from (Jones et al., 2019) for: A) Mt. Kring Holocene samples, B) Hughes Bluff samples with outliers identified and omitted using outlier detection in ice-tea.org.

The variation in thinning rates between Mt. Kring and Hughes Bluff is suggestive of past dynamic thinning rather than accumulation-driven outlet glacier changes. Previous work from inland sites similar to Mt Kring suggested that such sites changed little or may have thickened during the Holocene due to accumulation increases (Bockheim et al., 1989; Denton et al., 1989). In contrast, the synchronous timing but lower thinning rate observed at Mt Kring in this study suggests that this thinning was driven by ocean-ice sheet interactions at the coast that propagated inland. Such dynamic thinning, where increased ice-shelf basal melting and grounding line retreat leads to accelerated flow and inland thinning, is well documented along modern marine terminating margins of the Greenland and Antarctic ice sheets (Pritchard et al., 2009, 2012), yet identification in geologic record

is rare, primarily due to a lack of exposed bedrock in the upper reaches of glacier catchments. The thinning history from David Glacier allows for a unique comparison with the broad pattern of dynamic thinning derived from the modern satellite record and suggests dynamic thinning can occur >100 km into the interior of the EAIS and can persist over multiple-millennia.

3.5 Exposure age data - ice sheet model comparison

During the LGM, ice core records and numerical model outputs suggest that the EAIS experienced widespread thinning in its interior, while coastal sites experienced extensive thickening (Verleyen et al., 2011; Mackintosh et al., 2014). Our data from Mt Kring show that the ice sheet was thicker than present at this site during the LGM, and recorded ~200 metres of thinning during the Holocene. This provides a critical tie point between the high elevation, low accumulation ice domes where ice cores are drilled and the low elevation, high accumulation coastal sites with more abundant geologic data. Mt. Kring is the first site along the high elevation margin of the EAIS to constrain LGM ice sheet behavior and represents a unique site to compare with other ice sheet reconstructions and continental-scale ice sheet modelling experiments.

The chronologies from David Glacier provide critical insights to the rate, timing, style and magnitude of thinning from a marine based outlet glacier. The thinning histories presented here provide context to modelled continental-scale ice sheet reconstructions. Using the data-model comparison software (dmc.ICE-D.org), we extracted a modelled elevation history for David Glacier from five different ice sheet models (four continental-scale and one regional-catchment scale) and one ice sheet reconstruction created to drive a GIA model (Argus et al., 2014; Pollard et al., 2016, 2017, 2018; Kingslake et al., 2018; Lowry et al., 2019). In order to overcome differences in spatial resolution, the scheme extracts an interpolated ice elevation history from the model grid cell containing the field site and its neighbouring model grid cells. The suite of ice sheet models in which we compare against our geologic data, represent a variation in model grid size, flow approximations, model physics used, forcing and boundary conditions. We use these to provide a first order approximation for expected results from the ice sheet modelling community.

The resulting data-model comparison for Hughes Bluff and Mt. Kring reveal a noticeable mismatch in time during the main phase of thinning (Fig. 8). For Mt. Kring, ice sheet models indicate a phase of thinning that precedes our thinning history by ~4-7 kyr. For Hughes Bluff, the timing lag is comparable to Mt. Kring with one notable exception being the post glacial rebound model of ICE-6G. This improved match is likely because ICE-6G is constrained by multiple relative sea level curves along the Scott Coast (Baroni and Hall, 2004; Hall, 2009; Argus et al., 2014). The style of thinning is variable between models with noticeable short-lived pauses in thinning, mainly during the Antarctic Cold Reversal (~15-13 ka) (Pedro et al., 2016). Relative to Hughes Bluff, the magnitude of modelled elevation changes at Mt. Kring geometrically fit better with the surface exposure age data. At Mt. Kring, the average modelled thickness changes for all models in Fig. 8A is 190 m ± 117 m, which compares well with the 144 m thickness change derived from our ice thinning chronology. In contrast, at Hughes Bluff, we capture only 181 metres of thickness change and the average modelled thickness change for all models in Fig. 8B is 623 m ± 142 m. These comparisons suggest that our surface exposure ages capture more of the overall ice thinning at Mt. Kring than at Hughes Bluff. Overall, the data-model mismatch may be related to (1) individual topographic features/outcrops not being spatially resolved in the models, (2) limited constraints on ocean/atmosphere forcing (e.g. Lowry et al., 2019) and (3) poorly

constrained model parameters that influence basal sliding, isostatic adjustment and ice flow/rheology which impact the rate of ice sheet response to a climate forcing (Lowry et al., 2020; Kingslake et al., 2018).

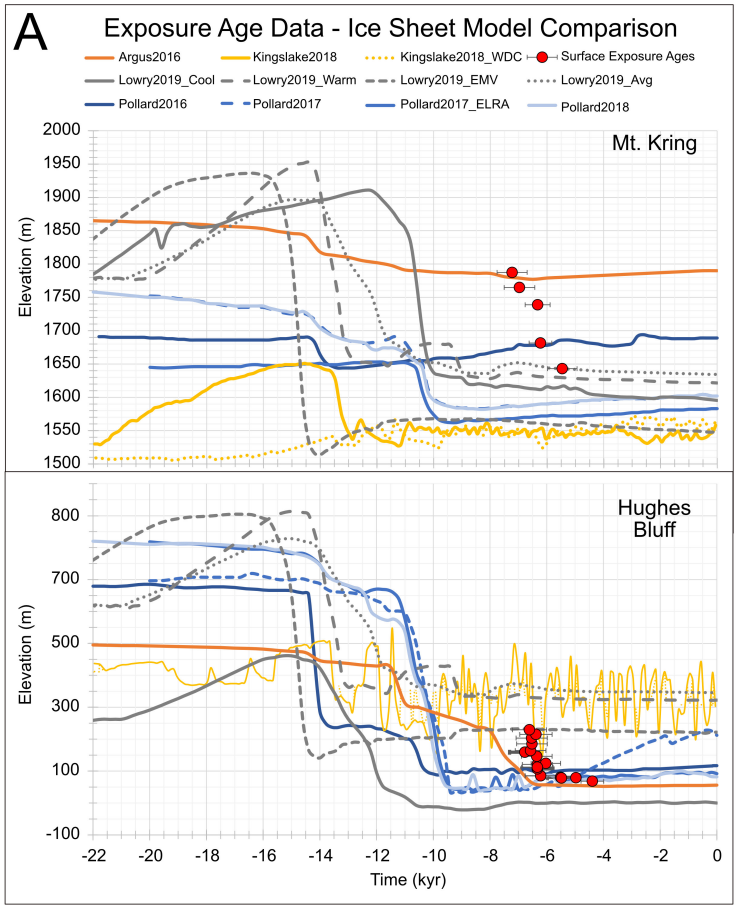

Figure 8. Surface exposure age data - ice sheet model comparisons for a) Mt. Kring and b) Hughes Bluff. Ice sheet modelled reconstruction data and supporting information from dmc.ice-d.org

4 Results - Deglacial sensitivity experiments

375 Based on the thinning histories presented in this study, the main episode of glacier thinning occurs during the mid-Holocene and captures >200 metres of glacier change along the David Glacier. This time period does not correlate with significant increases in atmospheric temperature or global mean sea level (e.g., Lambeck et al., 2014; Menviel et al., 2011; Liu et al., 2009), therefore, we ask: 1) What is the role of ocean heat in driving the observed glacier thinning and retreat? and 2) Given that ice from David Glacier coalesced with grounded ice in the Ross Sea, what impact does ice sheet buttressing have on the 380 timing and style of glacier thinning and retreat? The style and rate of modelled thinning and retreat from all experiments are compiled in Table 3. We note we carried out many more experiments than reported here and only those that show notable

changes are presented. While we do not force our simulations by any date specific reconstructions or proxy data, we co-view our model results against our geologic data to allow generalised time-varying geometric relationships to be compared.

Focusing solely on SIMR, a set of sensitivity experiments (M1-3) simulate the impacts of enhanced ocean heat on grounding line retreat (Fig. 9). Modern SIMR have been calculated along the Drygalski Ice Tongue with an average of -4.89 m/yr $\pm$ 3.38 m/yr (Wuite et al., 2009). For our experiments, we progressively increased SIMR until retreat is initiated. Threshold values represent this step-wise increase in SIMR. After a 7.5 kyr spin up period, a threshold SIMR of -11 m/yr achieves rapid grounding line retreat behaviour and is consistent with the modern grounding line position. For melt rates between -2 and -10 m/yr (exp M1, M2 respectively), grounding line retreat is rapid but the final grounding line remains pinned to the prominent sill at the mouth of the David Fjord. Final modelled surface reconstructions for experiments M1 and M2 place the upper ice surface $\sim$300 metres above the Hughes Bluff site, yet agree well with Mt. Kring data constraints. In the high melt case (M3), the grounding line position pauses at the sill for approximately 5 kyr. The final retreat phase from the sill to a modern position correlates with a final surface consistent with modern observations.

Focusing on LBR experiments (S1-3), we simulate the impacts of glacier-ice sheet decoupling on grounding line retreat, a scenario suggested from glacial geomorphic features in the western Ross Sea (Shipp et al., 1999; Halberstadt et al., 2016) (Fig. 10). After a 7.5 kyr model spin up period, ice shelf buttressing is incrementally reduced until retreat is initiated. Retreat occurs when lateral buttressing is reduced by 4%. Further ice shelf debuttressing by 40% retreats the modelled grounding line to near modern configuration, deep in the David Fjord. In both cases, the reduced buttressing forces rapid grounding line retreat to a prominent sill at the mouth of the David Fjord. In these scenarios, the resulting modelled upper ice surface remains above the Hughes Bluff site when the grounding line is pinned to the sill. At Mt. Kring, modelled rapid thinning is synchronous with Hughes Bluff yet, this simulation results in an unrealistic final surface elevation 100s of metres below observed modern surface elevation.

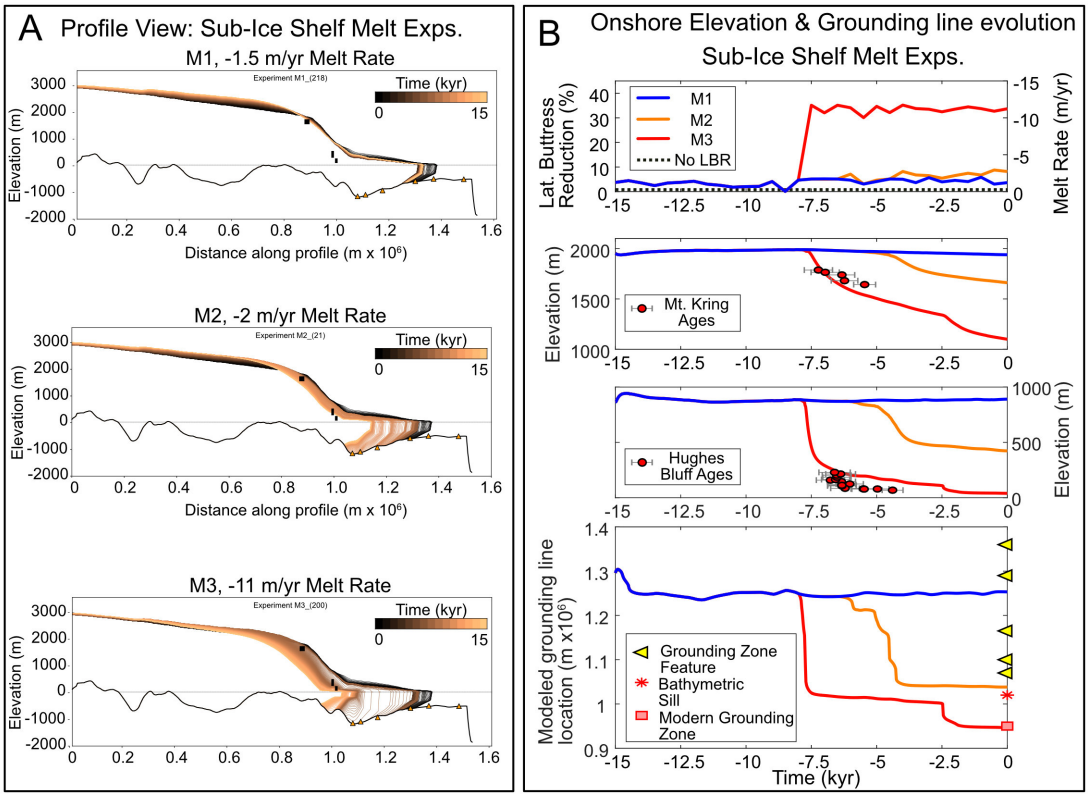

Figure 9. A) Profile View: 15 kyr evolution of modelled upper ice surface along flowline for sub-ice shelf melt rate (SIMR) experiments. Black bars represent elevation range from three sites in this study. Orange triangles represent offshore features marking observed grounding zone wedges. B) Onshore elevation and grounding line evolution for SIMR experiments. Top panel: Forcings applied, Top middle panel: Time-transgressive elevation profile for Mt. Kring with exposure ages, bottom middle panel: Time-transgressive elevation profile for Hughes Bluff surface exposure ages, and lower panel: Evolution of grounding line position with modern grounding line position, bathymetric sill at mouth of David Fjord and mapped grounding zone features. We co-view exposure age data in these plots to allow generalised time varying geometric relationships to be compared.

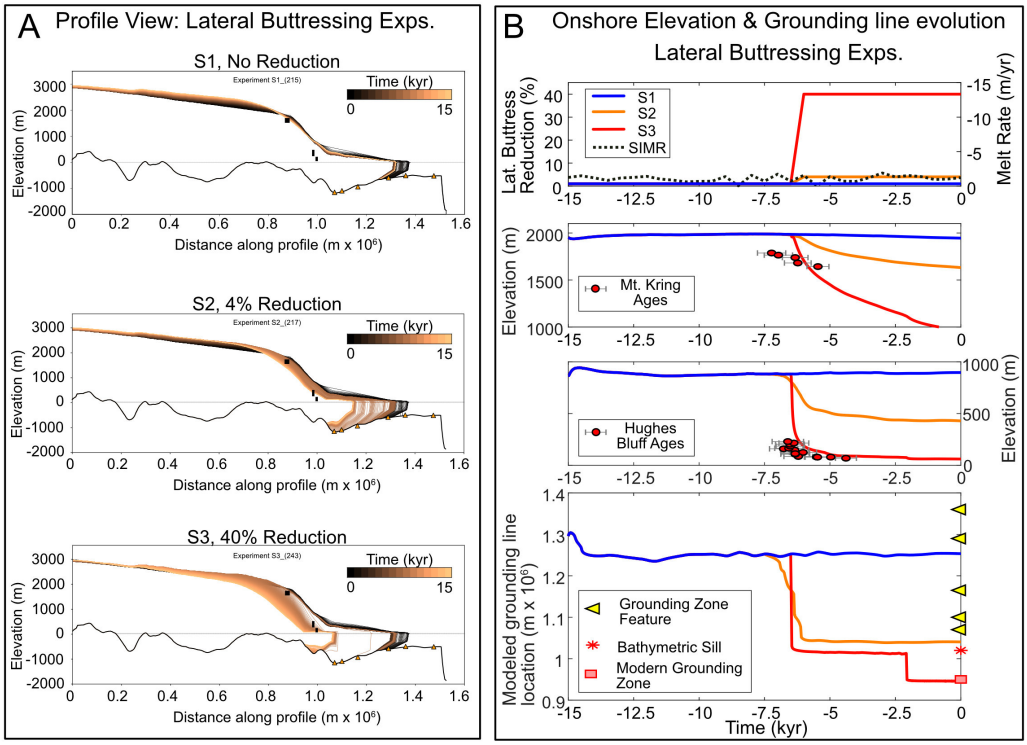

Figure 10. A) Profile View: 15 kyr evolution of modelled upper ice surface along flowline for lateral buttressing reduction (LBR) experiments. Black bars represent elevation range from three sites in this study. Orange triangles represent offshore features marking observed grounding zone wedges. B) Onshore elevation and grounding line evolution for LBR experiments. Top panel: Forcings applied, Top middle panel: Time-transgressive elevation profile for Mt. Kring with exposure ages, bottom middle panel: Time-transgressive elevation profile for Hughes Bluff surface exposure ages, and lower panel: Evolution of grounding line position with modern grounding line position, bathymetric sill at mouth of David Fjord and mapped grounding zone features. We co-view exposure age data in these plots to allow generalised time varying geometric relationships to be compared.

Finally, we force our model with a combination of SIMR and LBR. Our approach is similar to that used for individual forcings, except that this time we use a melt rate (MS1: -5 m/yr) and progressively reduce lateral buttressing until the grounding line retreats to near modern configuration. We then repeat this approach for two more cases of enhanced SIMR (MS2: -7 m/yr and MS3: -9 m/yr). Overall when forcings are combined, lower threshold values are required to initiate thinning and retreat (Fig. 11). For experiment MS3, the modelled upper ice surface reconstruction agrees well with the Mt. Kring chronology, yet Hughes Bluff remains ice covered until grounding line retreat from the sill approximately 5-6 kyr after the main phase of thinning and retreat.

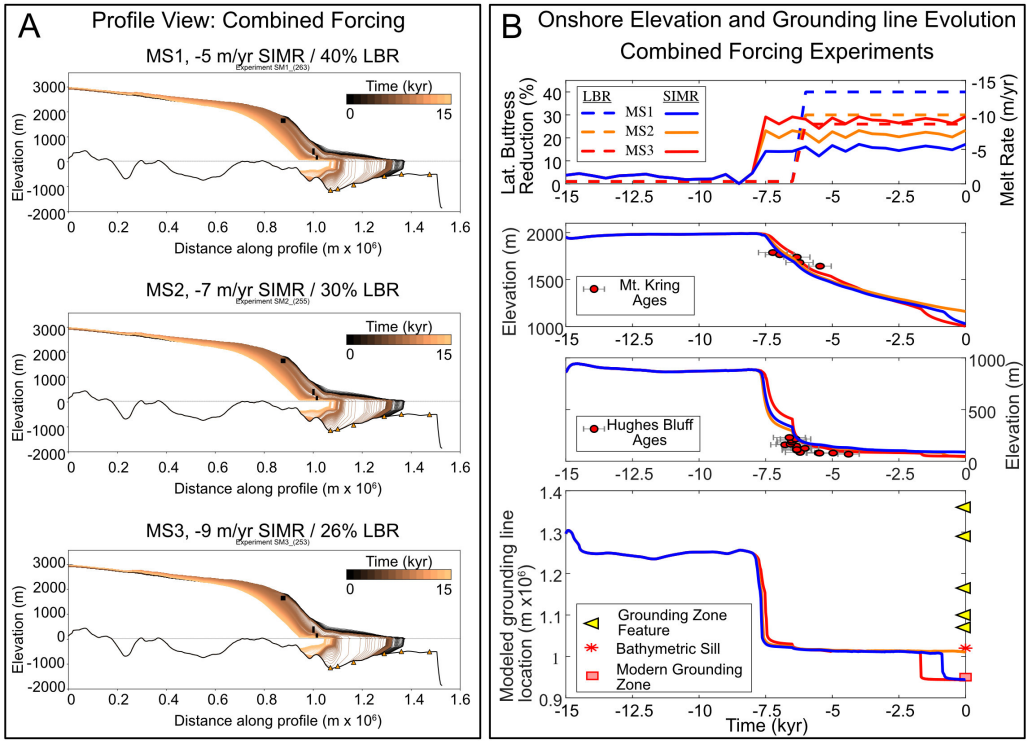

Figure 11. A) Profile View: 15 kyr evolution of modelled upper ice surface along flowline for combined forcing experiments. Black bars represent elevation range from three sites in this study. Orange triangles represent offshore features marking observed grounding zone wedges. B) Onshore elevation and grounding line evolution. Top panel: Forcings applied, Top middle panel: Time-transgressive elevation profile for Mt. Kring with exposure ages, bottom middle panel: Time-transgressive elevation profile for Hughes Bluff surface exposure ages, and lower panel: Evolution of grounding line position with modern grounding line position, bathymetric sill at mouth of David Fjord and mapped grounding zone features. We co-view exposure age data in these plots to allow generalised time varying geometric relationships to be compared.

We are confident that our modelling results reasonably reconstruct the period of multi-millennial glacial change during the mid-Holocene. However, our approach does have limitations including imperfect knowledge of past boundary conditions; treating ice as isothermal; lack of isostasy and subglacial hydrology paramterization; and no use of a calving law to control ice shelf length. Through modern sensitivity experiments, geologic control on geometry and a general fit to modern SIMR and basal stress, we remain confident our results support a first order approximation for the dominant controls on the David Glacier's thinning history.

Deglacial Experiment ID#	Modelled grounding line retreat behaviour	Modelled grounding line retreat rate (m/yr)	Modelled onshore glacier thinning behaviour	Max. Thinning @MK (m/yr)	Max. Thinning @HB (m/yr)
M1	Pinned near CI	0.44	Minimal thinning	0.20	0.15
M2	Rapid retreat to sill	356.50	Moderate thinning at HB, minmal atMK	0.20	0.58
M3	Two phase extreme retreat to modern GL position	620.60	Rapid runaway thinning at MK. Two phase rapid thinning above HB	1.02	8.73
S1	Pinned near CI	0.44	Minimal thinning	0.20	0.15
S2	Moderate retreat to sill	191.70	Moderate thinning at HB, minmal at MK	0.20	0.44
S3	Two phase retreat to modern GL position	331.70	Moderate runaway thinning at MK, rapid thinning above HB	0.44	2.37
MS1	Two phase moderate retreat to modern GL position	184.00	Moderate runaway thinning at MK, rapid thinning above HB	0.35	2.00
MS2	Two phase rapid retreat to modern GL position	397.80	Rapid runaway thinning at MK, two phase rapid thinning above HB	0.36	2.23
MS3	Two phase rapid retreat to modern GL position	489.30	Rapid runaway thinning at MK, two phase rapid thinning above HB	0.39	2.58

Table 3. Results for deglacial sensitivity experiments. We compare onshore and offshore modelled glacial behaviour, and thinning and grounding line retreat rates.

5 Discussion

The thinning history of David Glacier place modern observations in a long-term perspective and allows for local, regional and continent-wide comparisons with other glacial histories and modelled ice sheet reconstructions. High-resolution, low-inheritance exposure ages obtained from Hughes Bluff and Mt. Kring overlap in time, yet reveal different thinning styles with Hughes Bluff recording rapid ice surface lowering, and Mt. Kring revealing a much slower thinning signal. The chronology from Mt. Kring implies glacier thinning reached far inland along zones of streaming ice and provides rare constraints on ice behaviour from the margins of the EAIS.

The results of flowline modelling experiments along the expanded David Glacier reveal a threshold-driven sensitivity to both SIMR and ice stream lateral buttressing. Periods of modelled grounding line retreat match periods of onshore thinning constrained by surface exposure studies at two locations along the flowline. The results show the glacier response occurs at lower threshold values when the processes act in combination, consistent with previous applications of this model (Jamieson et al., 2014). Although the sensitivity experiments do not resolve which process or combination of processes forced the observed onshore thinning, we discuss potential explanations for our observed vs simulated relating to the thinning profile at Hughes Bluff and the data-model mismatch at Mt. Kring.

5.1 Coastal thinning and impacts on local oceanography

Continental-scale ice sheet model reconstructions and available geological data suggest that the glacier thinning profile at Hughes Bluff likely only captures the final 200 metres of the approximately 400+ metre thinning since the LGM (Fig. S2). In total, marine geological evidence, ice modelling and new results in this study suggest that at the LGM, the expanded David glacier had a surface profile above the level of Mt Kring and Hughes Bluff, and a stable grounding line location near Coulman Island (Licht et al., 1996; Domack et al., 1999; Shipp et al., 1999; McKay et al., 2008). Flowline modelling experiments starting from this ice extent and thickness capture both the magnitude and rate of onshore thinning derived from surface exposure data.

The new geological reconstruction of ice-surface elevation changes at Hughes Bluff shows a rapid lowering of the David Glacier at 6.5 ka and a period of slow thinning from ~6-4 ka. Given the marked slowdown in thinning rate from ~6 ka at Hughes Bluff (Figs 6B and 7B), we suggest that stabilisation of the Drygalski Ice Tongue occured after ~6 ka. Our modelling experiments reinforce this finding by showing that minimal ice surface lowering occurs once the grounding line retreats to a stable location near the modern grounding line location. Orombelli et al. (1990) and Baroni and Hall (2004) mapped a series of raised beaches along the TNB coastline that mark beach depositional processes in an open ocean setting (i.e. no grounded ice) initiating at 7.2 ka. Stevens et al. (2017a) highlight the influence of the Drygalski Ice Tongue on the local ocean conditions and development of the modern TNB Polynya. Evidence of the stability of the Drygalski Ice Tongue since ~6 ka from our surface exposure ages and modelling, along with the TNB raised beach chronology, suggests a strong connection betweeen modern and palaeo-oceanographic conditions highlighting he importance of the Drygalski Ice Tongue in development and sustained nature of the TNB polynya (Baroni and Hall, 2004; Stevens et al., 2017b; Mezgec et al., 2017).

5.2 Palaeo-thinning rate comparison

General agreement between palaeo-thinning rates derived from surface exposure ages of glacial deposits and those from our modelling experiments provide confidence in the approach used in this study. In Table 3, we show that in the combined forcing experiments, we achieve a close match between data-driven and glacier modelled thinning rates. For Hughes Bluff, a maximum thinning rate of 2.06 m/yr compares well with the average modelled thinning rate of 2.27 $\pm$ 0.29 m/yr (Exps. MS1-3). At Mt. Kring, maximum thinning rate is 0.19 $\pm$ 0.02 m/yr and, for experiments MS1-3, average modelled thinning rate of 0.36 m/yr.

Our modelling demonstrates that glacier thinning at Mt. Kring is sensitive to grounding line migration during ice retreat from the outer to the inner continental shelf. Mt. Kring is part of a broad bedrock platform along the northern flank of the major glacial trough dissecting the TAM (Fig. S1). The platform is comprised of three high elevation outcrops protruding ~200 metres above the ice, with Mt. Kring nearest to the zone of streaming ice (e.g. surface velocities >100 m/yr). Geophysical characterisation of the northern TAM suggests the presence of individual tectonic blocks bounded by faults which likely serve as zones of relatively weak rock strength allowing preferential ice flow and glacial erosion (Salvini and Storti, 1999; Dubbini et al., 2010). In West Antarctica, dynamic thinning of the inland ice sheet has been linked to underlying tectonic controls (Bingham et al., 2012). At David Glacier, similar tectonic controls may have conditioned the spatial pattern of dynamic thinning during the Holocene.

Along the upper reaches of the David Fjord, there are no outcrops in the zone of highest surface velocity (>100 m/yr). Mount Kring lies 40 km away from the modelled flowline, in an area of relatively slow flowing ice. Modern surface velocities near Mt. Kring are ∼15% of the surface velocities at the projected flowline position (Rignot et al., 2011). On modern ice sheets experiencing dynamic thinning, satellite derived thinning estimates are largest in the centre of the ice streams or outlet glaciers, and become progressively smaller at lower velocity sites further from the central flowline. For example, the central parts of Greenland's outlet glaciers are currently thinning at rates of ∼0.84 m/yr, while marginal areas with slower ice velocities are thinning at 0.12 m/yr (Pritchard et al., 2009). Therefore, it is likely that the Mt. Kring site likely reflects ice stream marginal thinning (maximum of 0.17 m/yr, derived from surface exposure data) rather than the greater thinning rate that was experienced in the centre of an ice stream (modelled maximum 0.3 m/yr). Taken together, the Hughes Bluff and Mt. Kring chronologies suggest that ∼2 kyr of dynamic thinning occurred at David Glacier, and that this thinning propagated significantly into the ice sheet interior.

5.3 Controls on thinning and grounding line migration

Overall, the style of modelled grounding line retreat is controlled by Marine Ice Sheet Instability, a positive feedback where grounding line retreat into overdeepened subglacial basins leading to progressively enhanced ice discharge and ice sheet thinning (Weertman et al., 1974; Mercer, 1978; Schoof, 2007). The topographic profile of the western Ross Sea is dominated by the deep and landward sloping Drygalski Trough and our modelling experiments show that the grounding line stabilises on a bathymetric sill at the mouth of the David Fjord. Experiments designed to simulate glacier-ice sheet decoupling show that once independent, the David Glacier grounding line rapidly retreats through the Dryglaski Trough to a pinning point near the TAM coastline.

This study provides insights into the processes that occurred as a large grounded section of an ice sheet retreated into discrete outlet glaciers. Previous descriptions of this retreat have focused on grounded ice in the Ross Sea as a whole (Licht et al., 1996; Shipp et al., 1999; Domack et al., 1999; McKay et al., 2008; Anderson et al., 2014). However, at the scale of David Glacier, retreat was likely influenced by local processes including interactions with adjacent glaciers and other ice bodies. For example, a recent ice sheet retreat reconstruction of Halberstadt et al. (2016) suggests that ice lingered on higher elevation banks as the grounding line retreated in adjacent, large bathymetric troughs. In reality, modelled grounding line retreat may have been slower due to lateral buttressing from outlet glaciers on the TAM coast and stagnant ice on bathymetric highs immediately seaward of the expanded David Glacier, and such lingering ice is not accounted for in our simplified modelling approach.

Knowledge of this complex lingering ice history is poorly constrained as the majority of research has focused on trough axes (Anderson et al., 2014; Halberstadt et al., 2016) whereas, offshore Mawson Glacier, south of David Glacier, sub-marine geomorphology reveals a complex record of lingering ice (Stutz, 2012; Greenwood et al., 2018; Prothro et al., 2020). Analysis of marine sediments, primarily from trough axes, indicate that a 'calving bay' environment formed during grounding line retreat (Domack et al., 1999, 2003; Leventer et al., 2006; Mackintosh et al., 2014). In this scenario, grounding line retreat is rapid along the trough axis while lingering ice remains grounded along the lateral margins of the ice stream/glacier. In addition to sedimentary evidence, the abundant large iceberg keelmarks seaward of the Coulman Island GZW and smaller keelmarks

within TNB provide evidence for a calving bay during deglaciation. Short-term grounding line stagnation may have been facilitated by complex interaction with other outlet glaciers (Reeves and Priestley glaciers together forming proto-Nansen Ice Sheet/Shelf) of TNB and/or grounded ice lingering on the banks surrounding the Drygalski Trough.

During the first ~500 model years, the modelled grounding line initially retreats to the location of a large grounding zone wedge (Lee, 2019). A lack of modelled grounding line stability at other, smaller GZWs suggests that the grounding-line may only have experienced short pauses in these locations. Further, in the case of the much smaller 'GZWs' observed in the deepest portion of the Drygalski Trough, the morphology may reflect a point source versus a line or zone source associated with more classically defined sheet-like GZWs. Regardless, the small mounds in the trough axis are likely to reflect short-lived grounding line pauses during overall retreat.

Generally, once initiated, the modelled David Glacier grounding line retreats rapidly and pauses at a prominent sill at the mouth of David Fjord for up to 5 kyr before subsequent grounding line retreat to its modern configuration. This simulated two-phase grounding line retreat compares well with our onshore reconstructions at Mt. Kring and Hughes Bluff, both in terms of timing and rates of past glacier thinning. Models forced by moderate SIMR and LBR, fit best with onshore geologic constraints.

Figure 12 synthesise the results of the terrestrial thinning chronology, modelled glacier flowline behaviour and the existing regional marine retreat chronologies. This synthesis suggests that beginning at 7.5 ka, with the grounding line pinned to the sill at the mouth of the David Fjord, the David Glacier and proto-Nansen Ice Shelf decouple and widespread onshore thinning is initiated. Between 6-5.5 ka, the grounding line retreats to near its modern position, thinning slows significantly and open marine conditions prevail regionally. In summary, evidence from offshore David Glacier indicates that retreat of grounded ice through the Drygalski Trough and the formation of open marine conditions similar to today occurred immediately prior to the dynamic thinning of David Glacier recorded in this study. Together with the existing retreat chronology outlined above, our onshore surface exposure data records the final stages of glacial thinning and retreat along the David Glacier and wider TNB area.

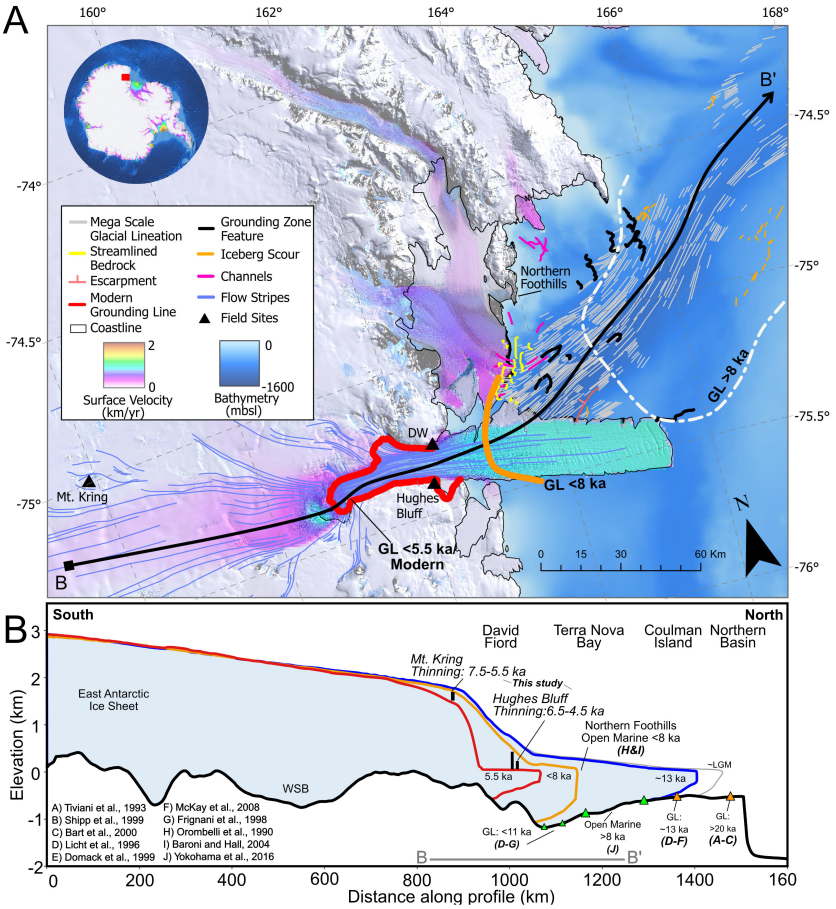

Figure 12. A) Map of David Glacier, Terra Nova Bay and surrounding areas. Synthesis map focused on two phase retreat between >8 ka and 5.5 ka, including geographic and geomorphic features mentioned in text. Surface velocity of (Rignot et al., 2011) and LIMA satellite data of (Bindschadler et al., 2008). Inset with red box for main extent shows bathymetry of (Arndt et al., 2013) and surface velocity of (Rignot et al., 2011). B) Synthesis profile focused on two phase retreat between 11 ka and 5.5 ka. Grounding zone features: triangles with age constraints (orange), triangles without age constraints (green) of Lee (2019). GL=Grounding line

6 Conclusions

Ice surface reconstructions from the David Glacier reveal a period of glacier thinning along a large swath of the drainage basin during the Mid-Holocene (∼6.5 ka). The reconstructed thinning style between two sites separated by ∼130 km, reveals a dynamic thinning event that endured for two millennia. This chronology is synchronous with local, regional and continental scale geological records of ice sheet behaviour yet is not fully captured in continental scale ice sheet models. Our flowline modelling results suggest that thinning and grounding-line retreat was driven by increased SIMR and decreased ice stream

lateral buttressing, and that the combination of these two processes reduces the individual forcing thresholds required to initiate retreat. Modelled episodes of grounding line retreat correlate well with periods of onshore thinning, constrained by our high-resolution surface exposure ages. Data-model mismatches likely highlight processes or feedbacks not represented in our simplified modelling approach related to the relative role of local topographic pinning points and the nature of ocean-forced dynamic thinning.

Through careful collection of glacial deposits from numerous sites along the David Glacier, we have closed a spatial and temporal gap in the rapidly expanding onshore glacial geologic knowledge bank. Our data constrain a 130 km portion of one of the largest outlet glaciers in the world which carries regional significance for Victoria Land and the western Ross Sea, as well as offering clues about processes currently underway in rapidly changing sectors of Antarctica and Greenland. While we acknowledge the data and modelling presented in this work may not apply to other settings, we hope that our study may serve as a template for future work aiming to extend the observations of ice sheet change beyond the last $\sim$40 years of satellite data.

Code availability. Modelling code

The code used for flowline modelling is available by request from the corresponding author.

Data availability. Geochemical data and exposure ages

Field, lab, analytical and exposure age data are available on ICE-D online database (antarctica.ICE-D.org) and in supplementary Tables 1-5

Sample availability. Samples collected during the 2016/17 austral summer are curated at Te Herenga Waka - Victoria University of Wellington and are available from the corresponding author. Samples collected prior to 2016/17 austral summer are curated at the University of Pisa.

Author contributions. JS contributed to project design, field work planning and implementation, sample analysis, modelling and preparation of manuscript. AM contributed to original project design, field work, modelling and manuscript preparation. KN contributed to original project design, sample analysis and manuscript preparation. RW contributed to field and lab work. CB and MCS led previous regional field work, contributed data and helped prepare manuscript. SC contributed to field and lab work. SJ led modelling work and contributed to preparation of manuscript. RSJ contributed to project design and modelling work. GB contributed to project design and BGC related lab work. PS contributed to Data-Model Comparison (DMC) work. JL contributed unpublished bathymetry data and regional marine geologic observations. YBS contributed to regional synthesis discussion. TW, LD, MI, FS, SIO, MC conducted AMS analyses at respective laboratories. LV

contributed through preparation of SfMP models, modelling and manuscript preparation. DL conributed to DMC work. RM contributed to regional marine geology synthesis.

Competing interests. The authors would like to declare that no competing interests are present

Acknowledgements. We would like to acknowledge NZARI (Grant 2017-1-3) for funding field work, AMS analyses and research visit to BGC. Support for a research visit to Durham University was provided by the Antarctic Science Bursary. We'd like to thank our trusty mountaineer Bia Boucinhas and pilot Mark Hayes for safe passage during field work. Logistical support for field and lab work was expertly provided by Antarctica New Zealand, Italian National Antarctic Programme (PNRA), Korean Polar Research Institute (KOPRI), Southern Lakes helicopters, Kenn Borek Air, Antarctic Research Centre , School of Geography, Earth and Environmental Studies, and Te Herenga Waka - Victoria University of Wellington. We extend a great deal of gratitude for the many experienced researchers in the David Glacier area for providing field photos from past expeditions.

References

Anderson, B. M., Hindmarsh, R. C., and Lawson, W. J.: A modelling study of the response of Hatherton Glacier to Ross Ice Sheet grounding line retreat, Global and Planetary Change, 42, 143–153, https://doi.org/10.1016/j.gloplacha.2003.11.006, 2004.

Anderson, J. B., Conway, H., Bart, P. J., Witus, A. E., Greenwood, S. L., McKay, R. M., Hall, B. L., Ackert, R. P., Licht, K., Jakobsson, M., and Stone, J. O.: Ross Sea paleo-ice sheet drainage and deglacial history during and since the LGM, Quaternary Science Reviews, 100, 31–54, https://doi.org/10.1016/j.quascirev.2013.08.020, 2014.

Andrews, J. T., Domack, E. W., Cunningham, W. L., Leventer, A., Licht, K. J., Jull, A. J. T., DeMaster, D. J., and Jennings, A. E.: Problems and Possible Solutions Concerning Radiocarbon Dating of Surface Marine Sediments, Ross Sea, Antarctica, Quaternary Research, 52, 206–216, https://doi.org/10.1006/qres.1999.2047, 1999.

Argus, D. F., Peltier, W. R., Drummond, R., and Moore, A. W.: The Antarctica component of postglacial rebound model ICE-6G_C (VM5a) based on GPS positioning, exposure age dating of ice thicknesses, and relative sea level histories, Geophysical Journal International, 198, 537–563, https://doi.org/10.1093/gji/ggu140, 2014.

Arndt, J. E., Schenke, H. W., Jakobsson, M., Nitsche, F. O., Buys, G., Goleby, B., Rebesco, M., Bohoyo, F., Hong, J., Black, J., Greku, R., Udintsev, G., Barrios, F., Reynoso-Peralta, W., Taisei, M., and Wigley, R.: The International Bathymetric Chart of the Southern Ocean (IBCSO) Version 1.0-A new bathymetric compilation covering circum-Antarctic waters, Geophysical Research Letters, 40, 3111–3117, https://doi.org/10.1002/grl.50413, 2013.

Arthern, R. J., Winebrenner, D. P., and Vaughan, D. G.: Antarctic snow accumulation mapped using polarization of 4.3-cm wavelength microwave emission, Journal of Geophysical Research Atmospheres, 111, D06 107, https://doi.org/10.1029/2004JD005667, 2006.

Atkins, C. B.: Geomorphological evidence of cold-based glacier activity in South Victoria Land, Antarctica, Geological Society, London, Special Publications, 381, 299–318, https://doi.org/10.1144/SP381.18, 2013.

Balco, G.: Contributions and unrealized potential contributions of cosmogenic-nuclide exposure dating to glacier chronology, 1990–2010, Quaternary Science Reviews, 30, 3–27, https://doi.org/10.1016/j.quascirev.2010.11.003, 2011.

Balco, G.: Technical note: A prototype transparent-middle-layer data management and analysis infrastructure for cosmogenic-nuclide exposure dating, Geochronology, 2, 169–175, https://doi.org/10.5194/gchron-2-169-2020, 2020.

Balco, G., Stone, J. O., Lifton, N. A., and Dunai, T. J.: A complete and easily accessible means of calculating surface exposure ages or erosion rates from 10Be and 26Al measurements, Quaternary Geochronology, 3, 174–195, https://doi.org/10.1016/J.QUAGEO.2007.12.001, https://www.sciencedirect.com/science/article/pii/S1871101407000647, 2008.

Balter-Kennedy, A., Bromley, G., Balco, G., Thomas, H., and Jackson, M. S.: A 14.5-million-year record of East Antarctic Ice Sheet fluctuations from the central Transantarctic Mountains, constrained with cosmogenic 3He, 10Be, 21Ne, and 26Al, The Cryosphere, 14, 2647–2672, https://doi.org/10.5194/tc-14-2647-2020, https://tc.copernicus.org/articles/14/2647/2020/, 2020.

Barletta, V. R., Bevis, M., Smith, B. E., Wilson, T., Brown, A., Bordoni, A., Willis, M., Khan, S. A., Rovira-Navarro, M., Dalziel, I., Smalley, R., Kendrick, E., Konfal, S., Caccamise, D. J., Aster, R. C., Nyblade, A., and Wiens, D. A.: Observed rapid bedrock uplift in Amundsen Sea Embayment promotes ice-sheet stability., Science (New York, N.Y.), 360, 1335–1339, https://doi.org/10.1126/science.aao1447, http://www.ncbi.nlm.nih.gov/pubmed/29930133, 2018.

Baroni, C. and Hall, B. L.: A new Holocene relative sea-level curve for Terra Nova Bay, Victoria Land, Antarctica, Journal of Quaternary Science, 19, 377–396, https://doi.org/10.1002/jqs.825, 2004.

Baroni, C., Frezzotti, M., Salvatore, M. C., Meneghel, M., Tabacco, I. E., Vittuari, L., Bondesan, A., Biasini, A., Cimbelli, A., and Orombelli, G.: Antarctic geomorphological and glaciological 1 : 250 000 map series: Mount Murchison quadrangle, northern Victoria Land. Explanatory notes, Annals of Glaciology, 39, 256–264, https://doi.org/10.3189/172756404781814131, 2004.

Bentley, M., Hein, A., Sugden, D., Whitehouse, P., Shanks, R., Xu, S., and Freeman, S.: Deglacial history of the Pensacola Mountains, Antarctica from glacial geomorphology and cosmogenic nuclide surface exposure dating, Quaternary Science Reviews, 158, 58–76, https://doi.org/10.1016/j.quascirev.2016.09.028, 2017.

Bentley, M. J., O Cofaigh, C., Anderson, J. B., Conway, H., Davies, B., Graham, A. G., Hillenbrand, C.-D., Hodgson, D. A., Jamieson, S. S., Larter, R. D., Mackintosh, A., Smith, J. A., Verleyen, E., Ackert, R. P., Bart, P. J., Berg, S., Brunstein, D., Canals, M., Colhoun, E. A., Crosta, X., Dickens, W. A., Domack, E., Dowdeswell, J. A., Dunbar, R., Ehrmann, W., Evans, J., Favier, V., Fink, D., Fogwill, C. J., Glasser, N. F., Gohl, K., Golledge, N. R., Goodwin, I., Gore, D. B., Greenwood, S. L., Hall, B. L., Hall, K., Hedding, D. W., Hein, A. S., Hocking, E. P., Jakobsson, M., Johnson, J. S., Jomelli, V., Jones, R. S., Klages, J. P., Kristoffersen, Y., Kuhn, G., Leventer, A., Licht, K., Lilly, K., Lindow, J., Livingstone, S. J., Massé, G., McGlone, M. S., McKay, R. M., Melles, M., Miura, H., Mulvaney, R., Nel, W., Nitsche, F. O., O'Brien, P. E., Post, A. L., Roberts, S. J., Saunders, K. M., Selkirk, P. M., Simms, A. R., Spiegel, C., Stolldorf, T. D., Sugden, D. E., van der Putten, N., van Ommen, T., Verfaillie, D., Vyverman, W., Wagner, B., White, D. A., Witus, A. E., and Zwartz, D.: A community-based geological reconstruction of Antarctic Ice Sheet deglaciation since the Last Glacial Maximum, Quaternary Science Reviews, 100, 1–9, https://doi.org/10.1016/j.quascirev.2014.06.025, 2014.

Bindschadler, R., Vornberger, P., Fleming, A., Fox, A., Mullins, J., Binnie, D., Paulsen, S., Granneman, B., and Gorodetsky, D.: The Landsat Image Mosaic of Antarctica, Remote Sensing of Environment, 112, 4214–4226, https://doi.org/10.1016/j.rse.2008.07.006, 2008.

Bingham, R. G., Ferraccioli, F., King, E. C., Larter, R. D., Pritchard, H. D., Smith, A. M., and Vaughan, D. G.: Inland thinning of West Antarctic Ice Sheet steered along subglacial rifts, Nature, 487, 468–471, https://doi.org/10.1038/nature11292, http://www.nature.com/articles/nature11292, 2012.

Blard, P.-H., Balco, G., Burnard, P., Farley, K., Fenton, C., Friedrich, R., Jull, A., Niedermann, S., Pik, R., Schaefer, J., Scott, E., Shuster, D., Stuart, F., Stute, M., Tibari, B., Winckler, G., and Zimmermann, L.: An inter-laboratory comparison of cosmogenic 3He and radiogenic 4He in the CRONUS-P pyroxene standard, Quaternary Geochronology, 26, 11–19, https://doi.org/10.1016/j.quageo.2014.08.004, 2015.

Bockheim, J. G., Wilson, S. C., Denton, G. H., Andersen, B. G. B. G., and Stuiver, M.: Late Quaternary ice-surface fluctuations of Hatherton Glacier, Transantarctic Mountains, Quaternary Research, 31, 229–254, https://doi.org/10.1016/0033-5894(89)90007-0, 1989.

Brancolini, G., Cooper, A. K., and Coren, F.: Seismic Facies and Glacial History in the Western Ross Sea (Antarctica), Geology and Seismic Stratigraphy of the Antarctic Margin, AGU Antarctic Research Series, 68, 209–233, 1995.

Bromley, G. R., Winckler, G., Schaefer, J. M., Kaplan, M. R., Licht, K. J., and Hall, B. L.: Pyroxene separation by HF leaching and its impact on helium surface-exposure dating, Quaternary Geochronology, 23, 1–8, https://doi.org/10.1016/J.QUAGEO.2014.04.003, https://www.sciencedirect.com/science/article/pii/S1871101414000351, 2014.

Buiron, D., Chappellaz, J., Stenni, B., Frezzotti, M., Baumgartner, M., Capron, E., Landais, A., Lemieux-Dudon, B., Masson-Delmotte, V., Montagnat, M., Parrenin, F., and Schilt, A.: TALDICE-1 age scale of the Talos Dome deep ice core, East Antarctica, Climate of the Past, 7, 1–16, https://doi.org/10.5194/cp-7-1-2011, 2011.

Cavitte, M. G. P., Parrenin, F., Ritz, C., Young, D. A., Van Liefferinge, B., Blankenship, D. D., Frezzotti, M., and Roberts, J. L.: Accumulation patterns around Dome C, East Antarctica, in the last 73 kyr, The Cryosphere, 12, 1401–1414, https://doi.org/10.5194/tc-12-1401-2018, https://www.the-cryosphere.net/12/1401/2018/, 2018.

Clark, P. U., Dyke, A. S., Shakun, J. D., Carlson, A. E., Clark, J., Wohlfarth, B., Mitrovica, J. X., Hostetler, S. W., and McCabe, A. M.: The Last Glacial Maximum., Science (New York, N.Y.), 325, 710–4, https://doi.org/10.1126/science.1172873, 2009.

Clason, C. C., Greenwood, S. L., Selmes, N., Lea, J. M., Jamieson, S. S. R., Nick, F. M., and Holmlund, P.: Controls on the early Holocene collapse of the Bothnian Sea Ice Stream, Journal of Geophysical Research: Earth Surface, 121, 2494–2513, https://doi.org/10.1002/2016JF004050, 2016.

Denton, G. H., Bockheim, J. G., Wilson, S. C., Leide, J. E., and Andersen, B. G.: Late Quaternary Ice-Surface Fluctuations of Beardmore Glacier, Transantarctic Mountains, Quaternary Research, 31, 183–209, https://doi.org/10.1016/0033-5894(89)90005-7, 1989.

Denton, G. H., Anderson, R. F., Toggweiler, J. R., Edwards, R. L., Schaefer, J. M., and Putnam, A. E.: The last glacial termination., Science (New York, N.Y.), 328, 1652–6, https://doi.org/10.1126/science.1184119, 2010.

Di Nicola, L., Strasky, S., Schlüchter, C., Salvatore, M. C., Akçar, N., Kubik, P. W., Christl, M., Kasper, H. U., Wieler, R., and Baroni, C.: Multiple cosmogenic nuclides document complex Pleistocene exposure history of glacial drifts in Terra Nova Bay (northern Victoria Land, Antarctica), Quaternary Research, 71, 83–92, https://doi.org/10.1016/j.yqres.2008.07.004, 2009.

Di Nicola, L., Baroni, C., Strasky, S., Salvatore, M. C., Schlüchter, C., Akçar, N., Kubik, P. W., and Wieler, R.: Multiple cosmogenic nuclides document the stability of the East Antarctic Ice Sheet in northern Victoria Land since the Late Miocene (5–7 Ma), Quaternary Science Reviews, 57, 85–94, https://doi.org/10.1016/j.quascirev.2012.09.026, 2012.

Domack, E., Leventer, A., Dunbar, R., Brachfeld, S., Manley, P., and McClennen, C.: Calving Bay Reentrants During the Late Pleistocene to Holocene Retreat of the Antarctic Ice Sheet: Sedimentologic and Geomorphologic Evidence, AGUFM, 2003, PP32D–07, https://ui.adsabs.harvard.edu/abs/2003AGUFMPP32D..07D/abstract, 2003.

Domack, E., Amblàs, D., Gilbert, R., Brachfeld, S., Camerlenghi, A., Rebesco, M., Canals, M., and Urgeles, R.: Subglacial morphology and glacial evolution of the Palmer deep outlet system, Antarctic Peninsula, Geomorphology, 75, 125–142, https://doi.org/10.1016/J.GEOMORPH.2004.06.013, 2006.

Domack, E. W., Jacobson, E. A., Shipp, S., and Anderson, J. B.: Late Pleistocene–Holocene retreat of the West Antarctic Ice-Sheet system in the Ross Sea: Part 2—Sedimentologic and stratigraphic signature, Geological Society of America Bulletin, 111, 1517, https://doi.org/10.1130/0016-7606(1999)111<1517:LPHROT>2.3.CO;2, https://pubs.geoscienceworld.org/gsabulletin/article/111/10/1517-1536/183433, 1999.

Dowdeswell, J. A., Cofaigh, C. O., and Pudsey, C. J.: Thickness and extent of the subglacial till layer beneath an Antarctic paleo–ice stream, Geology, 32, 13, https://doi.org/10.1130/G19864.1, https://pubs.geoscienceworld.org/geology/article/32/1/13-16/129195, 2004.

Dowdeswell, J. A., Canals, M., Jakobsson, M., Todd, B. J., Dowdeswell, E. K., and Hogan, K. A.: Introduction: an Atlas of Submarine Glacial Landforms, Geological Society, London, Memoirs, 46, 3–14, https://doi.org/10.1144/M46.171, 2016.

Dubbini, M., Cianfarra, P., Casula, G., Capra, A., and Salvini, F.: Active tectonics in northern Victoria Land (Antarctica) inferred from the integration of GPS data and geologic setting, Journal of Geophysical Research, 115, B12 421, https://doi.org/10.1029/2009JB007123, 2010.

Enderlin, E. M., Howat, I. M., and Vieli, A.: High sensitivity of tidewater outlet glacier dynamics to shape, The Cryosphere, 7, 1007–1015, https://doi.org/10.5194/tc-7-1007-2013, https://www.the-cryosphere.net/7/1007/2013/, 2013.

Fretwell, P., Pritchard, H. D., Vaughan, D. G., Bamber, J. L., Barrand, N. E., Bell, R., Bianchi, C., Bingham, R. G., Blankenship, D. D., Casassa, G., Catania, G., Callens, D., Conway, H., Cook, A. J., Corr, H. F. J., Damaske, D., Damm, V., Ferraccioli, F., Forsberg, R., Fujita, S., Gim, Y., Gogineni, P., Griggs, J. A., Hindmarsh, R. C. A., Holmlund, P., Holt, J. W., Jacobel, R. W., Jenkins, A., Jokat, W., Jordan, T., King, E. C., Kohler, J., Krabill, W., Riger-Kusk, M., Langley, K. A., Leitchenkov, G., Leuschen, C., Luyendyk, B. P., Matsuoka, K.,

Mouginot, J., Nitsche, F. O., Nogi, Y., Nost, O. A., Popov, S. V., Rignot, E., Rippin, D. M., Rivera, A., Roberts, J., Ross, N., Siegert, M. J., Smith, A. M., Steinhage, D., Studinger, M., Sun, B., Tinto, B. K., Welch, B. C., Wilson, D., Young, D. A., Xiangbin, C., and Zirizzotti, A.: Bedmap2: Improved ice bed, surface and thickness datasets for Antarctica, The Cryosphere, 7, 375–393, https://doi.org/10.5194/tc-7-375-2013, 2013.

Frezzotti, M., Pourchet, M., Flora, O., Gandolfi, S., Gay, M., Urbini, S., Vincent, C., Becagli, S., Gragnani, R., Proposito, M., Severi, M., Traversi, R., Udisti, R., and Fily, M.: Spatial and temporal variability of snow accumulation in East Antarctica from traverse data, Journal of Glaciology, 51, 2005.

Frignani, M., Giglio, F., Langone, L., Ravaioli, M., and Mangini, A.: Late Pleistocene-Holocene sedimentary fluxes of organic carbon and biogenic silica in the northwestern Ross Sea, Antarctica, Annals of Glaciology, 27, 697–703, https://doi.org/10.3189/1998AoG27-1-697-703, https://www.cambridge.org/core/product/identifier/S0260305500018280/type/journal_article, 1998.

Frisia, S., Weyrich, L. S., Hellstrom, J., Borsato, A., Golledge, N. R., Anesio, A. M., Bajo, P., Drysdale, R. N., Augustinus, P. C., Rivard, C., and Cooper, A.: The influence of Antarctic subglacial volcanism on the global iron cycle during the Last Glacial Maximum., Nature communications, 8, 15 425, https://doi.org/10.1038/ncomms15425, http://www.ncbi.nlm.nih.gov/pubmed/28598412http://www.pubmedcentral.nih.gov/articlerender.fcgi?artid=PMC5472753, 2017.

Giorgetti, G. and Baroni, C.: High-resolution analysis of silica and sulphate-rich rock varnishes from Victoria Land (Antarctica), European Journal of Mineralogy, 19, 381–389, https://doi.org/10.1127/0935-1221/2007/0019-1725, 2007.

Goehring, B. M., Balco, G., Todd, C., Moening-Swanson, I., and Nichols, K.: Late-glacial grounding line retreat in the northern Ross Sea, Antarctica, Geology, https://doi.org/10.1130/G45413.1, https://pubs.geoscienceworld.org/gsa/geology/article/568835/Lateglacial-grounding-line-retreat-in-the-northern, 2019.

Greenwood, S. L., Simkins, L. M., Halberstadt, A. R. W., Prothro, L. O., and Anderson, J. B.: Holocene reconfiguration and readvance of the East Antarctic Ice Sheet, Nature Communications, 9, 3176, https://doi.org/10.1038/s41467-018-05625-3, http://www.nature.com/articles/s41467-018-05625-3, 2018.

Halberstadt, A. R. W., Simkins, L. M., Greenwood, S. L., and Anderson, J. B.: Past ice-sheet behaviour: retreat scenarios and changing controls in the Ross Sea, Antarctica, The Cryosphere, 10, 1003–1020, https://doi.org/10.5194/tc-10-1003-2016, 2016.

Hall, B. L.: Holocene glacial history of Antarctica and the sub-Antarctic islands, Quaternary Science Reviews, 28, 2213–2230, https://doi.org/10.1016/j.quascirev.2009.06.011, 2009.

Howat, I. M., Porter, C., Smith, B. E., Noh, M.-J., and Morin, P.: The Reference Elevation Model of Antarctica, The Cryosphere, 13, 665–674, https://doi.org/10.5194/tc-13-665-2019, https://www.the-cryosphere.net/13/665/2019/, 2019.

IMBIE, T.: Mass balance of the Antarctic Ice Sheet from 1992 to 2017, Nature, 558, 219–222, https://doi.org/10.1038/s41586-018-0179-y, http://www.nature.com/articles/s41586-018-0179-y, 2018.

IPCC: Climate Change 2013: The Physical Science Basis. Contribution of Working Group I to the Fifth Assessment Report of the Intergovernmental Panel on Climate Change, Tech. rep., IPCC, 2013.

Jamieson, S. S. R., Vieli, A., Livingstone, S. J., Cofaigh, C. O., Stokes, C., Hillenbrand, C.-D., and Dowdeswell, J. A.: Ice-stream stability on a reverse bed slope, Nature Geoscience, 5, 799–802, https://doi.org/10.1038/NGEO1600, 2012.

Jamieson, S. S. R., Vieli, A., Cofaigh, C. O., Stokes, C. R., Livingstone, S. J., and Hillenbrand, C.-D.: Understanding controls on rapid ice-stream retreat during the last deglaciation of Marguerite Bay, Antarctica, using a numerical model, Journal of Geophysical Research: Earth Surface, 119, 247–263, https://doi.org/10.1002/2013JF002934, 2014.

Johnson, J. S., Hillenbrand, C.-D., Smellie, J. L., and Rocchi, S.: The last deglaciation of Cape Adare, northern Victoria Land, Antarctica, Antarctic Science, 20, 581, https://doi.org/10.1017/S0954102008001417, http://www.journals.cambridge.org/abstract_S0954102008001417, 2008.

Johnson, J. S., Bentley, M. J., Smith, J. A., Finkel, R. C., Rood, D. H., Gohl, K., Balco, G., Larter, R. D., and Schaefer, J. M.: Rapid Thinning of Pine Island Glacier in the Early Holocene, Science, 343, 2014.

Johnson, J. S., Smith, J. A., Schaefer, J. M., Young, N. E., Goehring, B. M., Hillenbrand, C.-D., Lamp, J. L., Finkel, R. C., and Gohl, K.: The last glaciation of Bear Peninsula, central Amundsen Sea Embayment of Antarctica: Constraints on timing and duration revealed by in situ cosmogenic 14C and 10Be dating, Quaternary Science Reviews, 178, 77–88, https://doi.org/10.1016/J.QUASCIREV.2017.11.003, https://www.sciencedirect.com/science/article/pii/S0277379116305364, 2017.

Johnson, J. S., Nichols, K. A., Goehring, B. M., Balco, G., and Schaefer, J. M.: Abrupt mid-Holocene ice loss in the western Weddell Sea Embayment of Antarctica, Earth and Planetary Science Letters, 518, 127–135, https://doi.org/10.1016/J.EPSL.2019.05.002, https://www.sciencedirect.com/science/article/pii/S0012821X19302638#ec0020, 2019.

Jones, R., Small, D., Cahill, N., Bentley, M., and Whitehouse, P.: iceTEA: Tools for plotting and analysing cosmogenic-nuclide surface-exposure data from former ice margins, Quaternary Geochronology, https://doi.org/10.1016/J.QUAGEO.2019.01.001, https://www.sciencedirect.com/science/article/pii/S1871101418301110, 2019.

Jones, R., Whitmore, R., Mackintosh, A., Norton, K., Eaves, S., Stutz, J., and Christl, M.: Regional-scale abrupt Mid-Holocene ice sheet thinning in the western Ross Sea, Antarctica, Geology, https://doi.org/10.1130/g48347.1, 2020.

Jones, R. S., Mackintosh, A. N., Norton, K. P., Golledge, N. R., Fogwill, C. J., Kubik, P. W., Christl, M., and Greenwood, S. L.: Rapid Holocene thinning of an East Antarctic outlet glacier driven by marine ice sheet instability, Nature Communications, 6, https://doi.org/10.1038/ncomms9910, 2015.

Jones, R. S., Gudmundsson, G. H., Mackintosh, A. N., McCormack, F. S., and Whitmore, R. J.: Ocean-Driven and Topography-Controlled Nonlinear Glacier Retreat During the Holocene: Southwestern Ross Sea, Antarctica, Geophysical Research Letters, 48, https://doi.org/10.1029/2020GL091454, 2021.

Joughin, I., Bamber, J. L., Scambos, T., Tulaczyk, S., Fahnestock, M., and MacAyeal, D. R.: Integrating satellite observations with modelling: basal shear stress of the Filcher-Ronne ice streams, Antarctica, Philosophical Transactions of the Royal Society A: Mathematical, Physical and Engineering Sciences, 364, 1795–1814, https://doi.org/10.1098/rsta.2006.1799, https://royalsocietypublishing.org/doi/10.1098/rsta.2006.1799, 2006.

Joy, K., Fink, D., Storey, B., and Atkins, C.: A 2 million year glacial chronology of the Hatherton Glacier, Antarctica and implications for the size of the East Antarctic Ice Sheet at the Last Glacial Maximum, Quaternary Science Reviews, 83, 46–57, https://doi.org/10.1016/j.quascirev.2013.10.028, 2014.

Kingslake, J., Scherer, R. P., Albrecht, T., Coenen, J., Powell, R. D., Reese, R., Stansell, N. D., Tulaczyk, S., Wearing, M. G., and Whitehouse, P. L.: Extensive retreat and re-advance of the West Antarctic Ice Sheet during the Holocene, Nature, 558, 430–434, https://doi.org/10.1038/s41586-018-0208-x, http://www.nature.com/articles/s41586-018-0208-x, 2018.

Lambeck, K., Rouby, H., Purcell, A., Sun, Y., and Sambridge, M.: Sea level and global ice volumes from the Last Glacial Maximum to the Holocene., Proceedings of the National Academy of Sciences of the United States of America, 111, 15 296–303, https://doi.org/10.1073/pnas.1411762111, 2014.

Lee, J. I.: Onshore to Offshore glacial reconstruction of Terra Nova Bay, Western Ross Sea, in: XIII International Symposium on Antarctic Earch Sciences: Workshop, KOPRI, Incheon, 2019.

Lee, J. I., McKay, R. M., Golledge, N. R., Yoon, H. I., Yoo, K.-C., Kim, H. J., and Hong, J. K.: Widespread persistence of expanded East Antarctic glaciers in the southwest Ross Sea during the last deglaciation, Geology, 45, 403–406, https://doi.org/10.1130/G38715.1, https://pubs.geoscienceworld.org/geology/article/45/5/403-406/207900, 2017.

Lenaerts, J. T. M., van den Broeke, M. R., van de Berg, W. J., van Meijgaard, E., and Kuipers Munneke, P.: A new, high-resolution surface mass balance map of Antarctica (1979-2010) based on regional atmospheric climate modeling, Geophysical Research Letters, 39, n/a–n/a, https://doi.org/10.1029/2011GL050713, http://doi.wiley.com/10.1029/2011GL050713, 2012.

Leventer, A., Domack, E., Dunbar, R., Pike, J., Stickley, C., Maddison, E., Brachfeld, S., Manley, P., and McClennen, C.: Marine sediment record from the East Antarctic margin reveals dynamics of ice sheet recession, GSA Today, 16, 4, https://doi.org/10.1130/GSAT01612A.1, ftp://rock.geosociety.org/pub/GSAToday/gt0612.pdf, 2006.

Licht, K. J. and Andrews, J. T.: The 14 C Record of Late Pleistocene Ice Advance and Retreat in the Central Ross Sea, Antarctica, Arctic, Antarctic, and Alpine Research, 34, 324, https://doi.org/10.2307/1552491, 2002.

Licht, K. J., Jennings, A. E., Andrews, J. T., and Williams, K. M.: Chronology of late Wisconsin ice retreat from the western Ross Sea, Antarctica, Geology, 24, 223–226, https://doi.org/10.1130/0091-7613(1996)024<0223:COLWIR>2.3.CO;2, 1996.

Lifton, N., Sato, T., and Dunai, T. J.: Scaling in situ cosmogenic nuclide production rates using analytical approximations to atmospheric cosmic-ray fluxes, Earth and Planetary Science Letters, 386, 149–160, https://doi.org/10.1016/J.EPSL.2013.10.052, https://www.sciencedirect.com/science/article/pii/S0012821X13006316, 2014.

Liu, Z., Otto-Bliesner, B. L., He, F., Brady, E. C., Tomas, R., Clark, P. U., Carlson, A. E., Lynch-Stieglitz, J., Curry, W., Brook, E., Erickson, D., Jacob, R., Kutzbach, J., and Cheng, J.: Transient simulation of last deglaciation with a new mechanism for bolling-allerod warming, Science, 325, 310–314, https://doi.org/10.1126/science.1171041, www.sciencemag.org/cgi/content/full/325/5938/306/DC1, 2009.

Livingstone, S. J., O Cofaigh, C., Stokes, C. R., Hillenbrand, C.-D., Vieli, A., and Jamieson, S. S.: Antarctic palaeo-ice streams, Earth-Science Reviews, 111, 90–128, https://doi.org/10.1016/j.earscirev.2011.10.003, 2012.

Livingstone, S. J., Stokes, C. R., Cofaigh, C., Hillenbrand, C. D., Vieli, A., Jamieson, S. S. R., Spagnolo, M., and Dowdeswell, J. A.: Subglacial processes on an Antarctic ice stream bed. 1: Sediment transport and bedform genesis inferred from marine geophysical data, Journal of Glaciology, 62, 270–284, https://doi.org/10.1017/jog.2016.18, 2016.

Lowry, D. P., Golledge, N. R., Bertler, N. A. N., Jones, R. S., and McKay, R.: Deglacial grounding-line retreat in the Ross Embayment, Antarctica, controlled by ocean and atmosphere forcing, Science Advances, 5, https://doi.org/10.1126/sciadv.aav8754, https://advances.sciencemag.org/lookup/doi/10.1126/sciadv.aav8754, 2019.

Lowry, D. P., Golledge, N. R., Bertler, N. A., Jones, R. S., McKay, R., and Stutz, J.: Geologic controls on ice sheet sensitivity to deglacial climate forcing in the Ross Embayment, Antarctica, Quaternary Science Advances, 1, 100 002, https://doi.org/10.1016/J.QSA.2020.100002, https://www.sciencedirect.com/science/article/pii/S2666033420300022, 2020.

MacGregor, J. A., Boisvert, L. N., Medley, B., Petty, A. A., Harbeck, J. P., Bell, R. E., Blair, J. B., Blanchard-Wrigglesworth, E., Buckley, E. M., Christoffersen, M. S., Cochran, J. R., Csathó, B. M., Marco, E. L. D., Dominguez, R. T., Fahnestock, M. A., Farrell, S. L., Gogineni, S. P., Greenbaum, J. S., Hansen, C. M., Hofton, M. A., Holt, J. W., Jezek, K. C., Koenig, L. S., Kurtz, N. T., Kwok, R., Larsen, C. F., Leuschen, C. J., Locke, C. D., Manizade, S. S., Martin, S., Neumann, T. A., Nowicki, S. M., Paden, J. D., Richter-Menge, J. A., Rignot, E. J., Rodríguez-Morales, F., Siegfried, M. R., Smith, B. E., Sonntag, J. G., Studinger, M., Tinto, K. J., Truffer, M., Wagner, T. P., Woods, J. E., Young, D. A., and Yungel, J. K.: The Scientific Legacy of NASA's Operation IceBridge, Reviews of Geophysics, 59, e2020RG000 712, https://doi.org/10.1029/2020RG000712,

https://agupubs.onlinelibrary.wiley.com/doi/full/10.1029/2020RG000712https://agupubs.onlinelibrary.wiley.com/doi/abs/10.1029/2020RG000712https://agupubs.onlinelibrary.wiley.com/doi/10.1029/2020RG000712, 2021.

Mackintosh, A., White, D., Fink, D., Gore, D. B., Pickard, J., and Fanning, P. C.: Exposure ages from mountain dipsticks in Mac. Robertson Land, East Antarctica, indicate little change in ice-sheet thickness since the Last Glacial Maximum, Geology, 35, 551, https://doi.org/10.1130/G23503A.1, 2007.

Mackintosh, A. N., Verleyen, E., O'Brien, P. E., White, D. A., Jones, R. S., McKay, R., Dunbar, R., Gore, D. B., Fink, D., Post, A. L., Miura, H., Leventer, A., Goodwin, I., Hodgson, D. A., Lilly, K., Crosta, X., Golledge, N. R., Wagner, B., Berg, S., van Ommen, T., Zwartz, D., Roberts, S. J., Vyverman, W., and Masse, G.: Retreat history of the East Antarctic Ice Sheet since the Last Glacial Maximum, Quaternary Science Reviews, 100, 10–30, https://doi.org/10.1016/J.QUASCIREV.2013.07.024, https://www.sciencedirect.com/science/article/pii/S0277379113002898, 2014.

Marrero, S. M., Phillips, F. M., Borchers, B., Lifton, N., Aumer, R., and Balco, G.: Cosmogenic nuclide systematics and the CRONUScalc program, Quaternary Geochronology, 31, 160–187, https://doi.org/10.1016/J.QUAGEO.2015.09.005, https://www.sciencedirect.com/science/article/pii/S1871101415300595, 2016.

McKay, R., Golledge, N. R., Maas, S., Naish, T., Levy, R., Dunbar, G., and Kuhn, G.: Antarctic marine ice-sheet retreat in the Ross Sea during the early Holocene, Geology, 44, 7–10, https://doi.org/10.1130/G37315.1, 2016.

McKay, R. M., Dunbar, G. B., Naish, T. R., Barrett, P. J., Carter, L., and Harper, M.: Retreat history of the Ross Ice Sheet (Shelf) since the Last Glacial Maximum from deep-basin sediment cores around Ross Island, Palaeogeography, Palaeoclimatology, Palaeoecology, 260, 245–261, https://doi.org/10.1016/j.palaeo.2007.08.015, 2008.

Menviel, L., Timmermann, A., Timm, O. E., and Mouchet, A.: Deconstructing the Last Glacial termination: The role of millennial and orbital-scale forcings, Quaternary Science Reviews, 30, 1155–1172, https://doi.org/10.1016/j.quascirev.2011.02.005, 2011.

Mercer, J. H.: West Antarctic ice sheet and CO2 greenhouse effect: a threat of disaster, Nature, 271, 321–325, https://doi.org/10.1038/271321a0, 1978.

Meredith, M., Sommerkorn, M., Cassotta, S., Derksen, C., Ekaykin, A., Hollowed, A., Kofinas, G., Mackintosh, A., Melbourne-Thomas, J., Muelbert, M., Ottersen, G., Pritchard, H., and Schuur, E.: Polar Regions. In: IPCC Special Report on the Ocean and Cryosphere in a Changing Climate [H.-O. Po¨rtner, D.C. Roberts, V. Masson-Delmotte, P. Zhai, M. Tignor, E. Poloczanska, K. Mintenbeck, A. Alegri´a, M. Nicolai, A. Okem, J. Petzold, B. Rama, N.M. Weye, Tech. rep., IPCC, https://www.ipcc.ch/srocc/chapter/chapter-3-2/, 2019.

Mezgec, K., Stenni, B., Crosta, X., Masson-Delmotte, V., Baroni, C., Braida, M., Ciardini, V., Colizza, E., Melis, R., Salvatore, M. C., Severi, M., Scarchilli, C., Traversi, R., Udisti, R., and Frezzotti, M.: Holocene sea ice variability driven by wind and polynya efficiency in the Ross Sea, Nature Communications, 8, 1–12, https://doi.org/10.1038/s41467-017-01455-x, 2017.

Miles, B. W. J., Stokes, C. R., Vieli, A., and Cox, N. J.: Rapid, climate-driven changes in outlet glaciers on the Pacific coast of East Antarctica, Nature, 500, 563–566, https://doi.org/10.1038/nature12382, 2013.

Morlighem, M., Rignot, E., Binder, T., Blankenship, D., Drews, R., Eagles, G., Eisen, O., Ferraccioli, F., Forsberg, R., Fretwell, P., and others: Deep glacial troughs and stabilizing ridges unveiled beneath the margins of the Antarctic ice sheet, Nature Geoscience, pp. 1–6, 2019.

Nichols, K. A., Goehring, B. M., Balco, G., Johnson, J. S., Hein, A. S., and Todd, C.: New Last Glacial Maximum ice thickness constraints for the Weddell Sea Embayment, Antarctica, The Cryosphere, 13, 2935–2951, https://doi.org/10.5194/tc-13-2935-2019, https://www.the-cryosphere.net/13/2935/2019/, 2019.

Nick, F. M., Vieli, A., Howat, I. M., and Joughin, I.: Large-scale changes in Greenland outlet glacier dynamics triggered at the terminus, Nature Geoscience, 2, 110–114, https://doi.org/10.1038/NGEO394, 2009.

Nick, F. M., Van Der Veen, C. J., Vieli, A., and Benn, D. I.: A physically based calving model applied to marine outlet glaciers and implications for the glacier dynamics, Journal of Glaciology, 56, 781–794, https://doi.org/10.3189/002214310794457344, 2010.

Norton, K. P., von Blanckenburg, F., Schlunegger, F., Schwab, M., and Kubik, P. W.: Cosmogenic nuclide-based investigation of spatial erosion and hillslope channel coupling in the transient foreland of the Swiss Alps, Geomorphology, 95, 474–486, https://doi.org/10.1016/J.GEOMORPH.2007.07.013, https://www.sciencedirect.com/science/article/pii/S0169555X07003509, 2008.

O Cofaigh, C., Dowdeswell, J. A., Allen, C. S., Hiemstra, J. F., Pudsey, C. J., Evans, J., and J.A. Evans, D.: Flow dynamics and till genesis associated with a marine-based Antarctic palaeo-ice stream, Quaternary Science Reviews, 24, 709–740, https://doi.org/10.1016/J.QUASCIREV.2004.10.006, https://www.sciencedirect.com/science/article/abs/pii/S0277379104003014, 2005.

Oberholzer, P., Baroni, C., Schaefer, J., Orombelli, G., Ochs, S. I., W., K. P., Baur, H., and Wieler, R.: Limited Pliocene/Pleistocene glaciation in Deep Freeze Range, northern Victoria Land, Antarctica, derived from in situ cosmogenic nuclides, Antarctic Science, 15, 493–502, https://doi.org/10.1017/S0954102003001603, 2003.

Oberholzer, P., Baroni, C., Salvatore, M., Baur, H., and Wieler, R.: Dating late Cenozoic erosional surfaces in Victoria Land, Antarctica, with cosmogenic neon in pyroxenes, Antarctic Science, 20, https://doi.org/10.1017/S095410200700079X, 2008.

Orombelli, G., Baroni, C., and Denton, G. H.: Late Cenozoic Glacial History of the Terra Nova Bay Region, Northern Victoria Land, Antarctica, Geografia Fisica e Dinamica Quaternaria, 13, 139–163, 1990.

Paxman, G. J., Jamieson, S. S., Hochmuth, K., Gohl, K., Bentley, M. J., Leitchenkov, G., and Ferraccioli, F.: Reconstructions of Antarctic topography since the Eocene–Oligocene boundary, Palaeogeography, Palaeoclimatology, Palaeoecology, 535, 109 346, https://doi.org/10.1016/J.PALAEO.2019.109346, https://www.sciencedirect.com/science/article/pii/S0031018219304845, 2019.

Pedro, J. B., Bostock, H. C., Bitz, C. M., He, F., Vandergoes, M. J., Steig, E. J., Chase, B. M., Krause, C. E., Rasmussen, S. O., Markle, B. R., and Cortese, G.: The spatial extent and dynamics of the Antarctic Cold Reversal, Nature Geoscience, 9, 51–55, https://doi.org/10.1038/ngeo2580, http://www.nature.com/articles/ngeo2580, 2016.

Pollard, D., Chang, W., Haran, M., Applegate, P., and DeConto, R.: Large ensemble modeling of the last deglacial retreat of the West Antarctic Ice Sheet: comparison of simple and advanced statistical techniques, Geoscientific Model Development, 9, 1697–1723, https://doi.org/10.5194/gmd-9-1697-2016, https://www.geosci-model-dev.net/9/1697/2016/, 2016.

Pollard, D., Gomez, N., and Deconto, R. M.: Variations of the Antarctic Ice Sheet in a Coupled Ice Sheet-Earth-Sea Level Model: Sensitivity to Viscoelastic Earth Properties, Journal of Geophysical Research: Earth Surface, 122, 2124–2138, https://doi.org/10.1002/2017JF004371, http://doi.wiley.com/10.1002/2017JF004371, 2017.

Pollard, D., Gomez, N., DeConto, R. M., and Han, H. K.: Estimating Modern Elevations of Pliocene Shorelines Using a Coupled Ice Sheet-Earth-Sea Level Model, Journal of Geophysical Research: Earth Surface, 123, 2279–2291, https://doi.org/10.1029/2018JF004745, https://onlinelibrary.wiley.com/doi/abs/10.1029/2018JF004745, 2018.

Pritchard, H. D., Arthern, R. J., Vaughan, D. G., and Edwards, L. A.: Extensive dynamic thinning on the margins of the Greenland and Antarctic ice sheets, Nature, 461, 971–975, https://doi.org/10.1038/nature08471, http://www.nature.com/articles/nature08471, 2009.

Pritchard, H. D., Ligtenberg, S. R. M., Fricker, H. A., Vaughan, D. G., van den Broeke, M. R., and Padman, L.: Antarctic ice-sheet loss driven by basal melting of ice shelves, Nature, 484, 502–505, https://doi.org/10.1038/nature10968, http://www.nature.com/articles/nature10968, 2012.

Prothro, L. O., Majewski, W., Yokoyama, Y., Simkins, L. M., Anderson, J. B., Yamane, M., Miyairi, Y., and Ohkouchi, N.: Timing and pathways of East Antarctic Ice Sheet retreat, Quaternary Science Reviews, 230, 106 166, https://doi.org/10.1016/J.QUASCIREV.2020.106166, https://www.sciencedirect.com/science/article/pii/S0277379119307024?casa_token=1bVC0-QUiZoAAAAA:mn3NgwF4MYiZqKyLcJZRF6czD-vLv9YBeDibp7_EHJFv47GjAbhi2cJh0v3kP2XsMZEG6xWlgoE#fig1, 2020.

Rhee, H. H., Lee, M. K., Seong, Y. B., Hong, S., Lee, J. I., Yoo, K.-C., and Yu, B. Y.: Timing of the local last glacial maximum in Terra Nova Bay, Antarctica defined by cosmogenic dating, Quaternary Science Reviews, 221, 105 897, https://doi.org/10.1016/J.QUASCIREV.2019.105897, https://www.sciencedirect.com/science/article/pii/S0277379119303373#fig6, 2019.

Rignot, E., Mouginot, J., and Scheuchl, B.: Ice flow of the Antarctic ice sheet., Science (New York, N.Y.), 333, 1427–30, https://doi.org/10.1126/science.1208336, 2011.

Rignot, E., Mouginot, J., Scheuchl, B., Broeke, M. v. d., Wessem, M. J. v., and Morlighem, M.: Four decades of Antarctic Ice Sheet mass balance from 1979–2017, Proceedings of the National Academy of Sciences, 116, 1095–1103, https://doi.org/10.1073/PNAS.1812883116, https://www.pnas.org/content/116/4/1095, 2019.

Rosenheim, B. E., Santoro, J. A., Gunter, M., and Domack, E. W.: Improving Antarctic Sediment 14C Dating Using Ramped Pyrolysis: An Example from the Hugo Island Trough, Radiocarbon, 55, 115–126, https://doi.org/10.1017/s0033822200047846, 2013.

Salvini, F. and Storti, F.: Cenozoic tectonic lineaments of the Terra Nova Bay region, Ross Embayment, Antarctica, Global and Planetary Change, 23, 129–144, https://doi.org/10.1016/S0921-8181(99)00054-5, https://www.sciencedirect.com/science/article/pii/S0921818199000545, 1999.

Schoof, C.: Ice sheet grounding line dynamics: Steady states, stability, and hysteresis, Journal of Geophysical Research: Earth Surface, 112, 1–19, https://doi.org/10.1029/2006JF000664, 2007.

Schroeder, D. M., Bingham, R. G., Blankenship, D. D., Christianson, K., Eisen, O., Flowers, G. E., Karlsson, N. B., Koutnik, M. R., Paden, J. D., and Siegert, M. J.: Five decades of radioglaciology, Annals of Glaciology, 61, 1–13, https://doi.org/10.1017/AOG.2020.11, https://www.cambridge.org/core/journals/annals-of-glaciology/article/five-decades-of-radioglaciology/BB862CCC314A993C14B3C6F62BD4F0B6, 2020.

Shipp, S., Anderson, J. B., Domack, E. W., Jacobson, E. A., Shipp, S., and Anderson, J. B.: Late Pleistocene–Holocene retreat of the West Antarctic Ice-Sheet system in the Ross Sea: Part 1—Geophysical results, GSA Bulletin, 111, 1517–1536, https://doi.org/10.1130/0016-7606(1999)111<1486:LPHROT>2.3.CO;2, 1999.

Siegert, M. J.: Glacial–interglacial variations in central East Antarctic ice accumulation rates, Quaternary Science Reviews, 22, 741–750, https://doi.org/10.1016/S0277-3791(02)00191-9, https://www.sciencedirect.com/science/article/pii/S0277379102001919, 2003.

Small, D., Bentley, M. J., Jones, R. S., Pittard, M. L., and Whitehouse, P. L.: Antarctic ice sheet palaeo-thinning rates from vertical transects of cosmogenic exposure ages, Quaternary Science Reviews, 206, 65–80, https://doi.org/10.1016/J.QUASCIREV.2018.12.024, https://www.sciencedirect.com/science/article/pii/S0277379118307728, 2019.

Smellie, J. L., Rocchi, S., Johnson, J. S., Di Vincenzo, G., and Schaefer, J. M.: A tuff cone erupted under frozen-bed ice (northern Victoria Land, Antarctica): linking glaciovolcanic and cosmogenic nuclide data for ice sheet reconstructions, Bulletin of Volcanology, 80, 12, https://doi.org/10.1007/s00445-017-1185-x, http://link.springer.com/10.1007/s00445-017-1185-x, 2018.

Spector, P., Stone, J., Cowdery, S. G., Hall, B., Conway, H., and Bromley, G.: Rapid Early-Holocene Deglaciation in the Ross Sea, Antarctica, Geophysical Research Letters, https://doi.org/10.1002/2017GL074216, http://doi.wiley.com/10.1002/2017GL074216, 2017.

Stern, T., Baxter, A., and Barrett, P.: Isostatic rebound due to glacial erosion within the Transantarctic Mountains, Geology, 33, 221, https://doi.org/10.1130/G21068.1, 2005.

Stevens, C., Fusco, G., Yun, S., Grant, B., Robinson, N., and Hwang, C. Y.: The influence of the Drygalski Ice Tongue on the local ocean, https://doi.org/10.1017/aog.2017.4, 2017a.

Stevens, C., Sang Lee, W., Fusco, G., Yun, S., Grant, B., Robinson, N., and Yeon Hwang, C.: The influence of the Drygalski Ice Tongue on the local ocean, Annals of Glaciology, 58, 51–59, https://doi.org/10.1017/aog.2017.4, https://www.cambridge.org/core/product/identifier/S0260305517000040/type/journal_article, 2017b.

Stokes, C. R., Tarasov, L., Blomdin, R., Cronin, T. M., Fisher, T. G., Gyllencreutz, R., Hättestrand, C., Heyman, J., Hindmarsh, R. C., Hughes, A. L., Jakobsson, M., Kirchner, N., Livingstone, S. J., Margold, M., Murton, J. B., Noormets, R., Peltier, W. R., Peteet, D. M., Piper, D. J., Preusser, F., Renssen, H., Roberts, D. H., Roche, D. M., Saint-Ange, F., Stroeven, A. P., and Teller, J. T.: On the reconstruction of palaeo-ice sheets: Recent advances and future challenges, Quaternary Science Reviews, 125, 15–49, https://doi.org/10.1016/J.QUASCIREV.2015.07.016, https://www.sciencedirect.com/science/article/pii/S027737911530055X, 2015.

Stone, J. O., Balco, G. A., Sugden, D. E., Caffee, M. W., Sass, L. C., Cowdery, S. G., and Siddoway, C.: Holocene deglaciation of Marie Byrd Land, West Antarctica., Science (New York, N.Y.), 299, 99–102, https://doi.org/10.1126/science.1077998, 2003.

Stuiver, M., Denton, G., Hughes, T., and Fastook, J.: History of the Marine Ice Sheet in West Antarctic during the Last Glaciation: A working hypothesis, in: The Last Great Ice Sheets, edited by Denton, G. H. and Hughes, T., pp. 319–369, Wiley, New York, 1981.

Stutz, J.: Reconstruction of LGM and Post LGM Glacial Environment of McMurdo Sound: Implications for Ice Dynamics, Depositional Systems and Glacial Isostatic Adjustment, Ph.D. thesis, The Ohio State University, 2012.

Sugden, D. E., Balco, G., Cowdery, S. G., Stone, J. O., and Sass, L. C.: Selective glacial erosion and weathering zones in the coastal mountains of Marie Byrd Land, Antarctica, Geomorphology, 67, 317–334, https://doi.org/10.1016/J.GEOMORPH.2004.10.007, https://www.sciencedirect.com/science/article/pii/S0169555X04002582, 2005.

Todd, C., Stone, J., Conway, H., Hall, B., and Bromley, G.: Late Quaternary evolution of Reedy Glacier, Antarctica, Quaternary Science Reviews, 29, 1328–1341, https://doi.org/10.1016/j.quascirev.2010.02.001, 2010.

van Wessem, J. M., van de Berg, W. J., Noël, B. P. Y., van Meijgaard, E., Amory, C., Birnbaum, G., Jakobs, C. L., Krüger, K., Lenaerts, J. T. M., Lhermitte, S., Ligtenberg, S. R. M., Medley, B., Reijmer, C. H., van Tricht, K., Trusel, L. D., van Ulft, L. H., Wouters, B., Wuite, J., and van den Broeke, M. R.: Modelling the climate and surface mass balance of polar ice sheets using RACMO2 – Part 2: Antarctica (1979–2016), The Cryosphere, 12, 1479–1498, https://doi.org/10.5194/tc-12-1479-2018, https://www.the-cryosphere.net/12/1479/2018/, 2018.

Vargo, L. J., Anderson, B. M., Horgan, H. J., Mackintosh, A. N., Lorrey, A. M., and Thornton, M.: Using structure from motion photogrammetry to measure past glacier changes from historic aerial photographs, Journal of Glaciology, 63, 1105–1118, https://doi.org/10.1017/jog.2017.79, https://www.cambridge.org/core/product/identifier/S002214301700079X/type/journal_article, 2017.

Veres, D., Bazin, L., Landais, A., Toyé Mahamadou Kele, H., Lemieux-Dudon, B., Parrenin, F., Martinerie, P., Blayo, E., Blunier, T., Capron, E., Chappellaz, J., Rasmussen, S. O., Severi, M., Svensson, A., Vinther, B., and Wolff, E. W.: The Antarctic ice core chronology (AICC2012): an optimized multi-parameter and multi-site dating approach for the last 120 thousand years, Climate of the Past, 9, 1733–1748, https://doi.org/10.5194/cp-9-1733-2013, https://www.clim-past.net/9/1733/2013/, 2013.

Verleyen, E., Hodgson, D. A., Sabbe, K., Cremer, H., Emslie, S. D., Gibson, J., Hall, B., Imura, S., Kudoh, S., Marshall, G. J., McMinn, A., Melles, M., Newman, L., Roberts, D., Roberts, S. J., Singh, S. M., Sterken, M., Tavernier, I., Verkulich, S., de Vyver, E. V., Van Nieuwenhuyze, W., Wagner, B., and Vyverman, W.: Post-glacial regional climate variability along the East

Antarctic coastal margin—Evidence from shallow marine and coastal terrestrial records, Earth-Science Reviews, 104, 199–212, https://doi.org/10.1016/J.EARSCIREV.2010.10.006, https://www.sciencedirect.com/science/article/pii/S0012825210001418, 2011.

Vieli, A. and Payne, A. J.: Assessing the ability of numerical ice sheet models to simulate grounding line migration, Journal of Geophysical Research: Earth Surface, 110, F01 003, https://doi.org/10.1029/2004JF000202, 2005.

Weber, M. E., Clark, P. U., Kuhn, G., Timmermann, A., Sprenk, D., Gladstone, R., Zhang, X., Lohmann, G., Menviel, L., Chikamoto, M. O., Friedrich, T., and Ohlwein, C.: Millennial-scale variability in Antarctic ice-sheet discharge during the last deglaciation, Nature, 510, 134–138, https://doi.org/10.1038/nature13397, http://www.nature.com/articles/nature13397, 2014.

Weertman, J., Bentley, C. R., and Walker, J. C. F.: Stability of the Junction of an Ice Sheet and an Ice Shelf, Journal of Glaciology, 13, 3–11, https://doi.org/10.1017/S0022143000023327, 1974.

White, D. A., Fink, D., and Gore, D. B.: Cosmogenic nuclide evidence for enhanced sensitivity of an East Antarctic ice stream to change during the last deglaciation, Geology, 39, 23–26, https://doi.org/10.1130/G31591.1, https://pubs.geoscienceworld.org/geology/article/39/1/23-26/130375, 2011.

Whitehouse, P. L., Bentley, M. J., and Le Brocq, A. M.: A deglacial model for Antarctica: geological constraints and glaciological modelling as a basis for a new model of Antarctic glacial isostatic adjustment, Quaternary Science Reviews, 32, 1–24, https://doi.org/10.1016/j.quascirev.2011.11.016, 2012.

Whitehouse, P. L., Bentley, M. J., Vieli, A., Jamieson, S. S. R., Hein, A. S., and Sugden, D. E.: Controls on Last Glacial Maximum ice extent in the Weddell Sea embayment, Antarctica, Journal of Geophysical Research: Earth Surface, 122, 371–397, https://doi.org/10.1002/2016JF004121, 2017.

Whitehouse, P. L., Gomez, N., King, M. A., and Wiens, D. A.: Solid Earth change and the evolution of the Antarctic Ice Sheet, Nature Communications, 10, 503, https://doi.org/10.1038/s41467-018-08068-y, http://www.nature.com/articles/s41467-018-08068-y, 2019.

Wuite, J., Jezek, K. C., Wu, X., Farness, K., and Carande, R.: The velocity field and flow regime of David Glacier and Drygalski Ice Tongue, Antarctica, Polar Geography, 32, 111–127, https://doi.org/10.1080/10889370902815499, 2009.

Yokoyama, Y., Anderson, J. B., Yamane, M., Simkins, L. M., Miyairi, Y., Yamazaki, T., Koizumi, M., Suga, H., Kusahara, K., Prothro, L., Hasumi, H., Southon, J. R., and Ohkouchi, N.: Widespread collapse of the Ross Ice Shelf during the late Holocene, PNAS, 113, 2354–2359, https://doi.org/10.1073/pnas.1516908113, 2016.

Zoet, L. K., Anandakrishnan, S., Alley, R. B., Nyblade, A. A., and Wiens, D. A.: Motion of an Antarctic glacier by repeated tidally modulated earthquakes, Nature Geoscience, 5, 623–626, https://doi.org/10.1038/NGEO1555, 2012.